Contract No:

This document was prepared in conjunction with work accomplished under Contract No. 89303321CEM000080 with the U.S. Department of Energy (DOE) Office of Environmental Management (EM).

Disclaimer:

Functionalized Mesoporous Carbon and Silica for Effective Recovery of Rare Earth Elements from Magnet Scrap

Proposal Number: WP22-S1-3463
Lead PI: Dien Li
Lead Organization: Savannah River National Laboratory, Aiken, SC 29808
Date: December 1, 2022
Version: 0

Table of Contents

List of Tables

List of Figures

List of Acronyms

Acronym	Meaning
ARPA-E	Advanced Research Project Agency-Energy
APTS	3-Aminopropyl)triethoxysilane
BET	Brunauer–Emmett–Teller
CLS	Canadian Light Source
CMK	Carbon mesostructured by KAIST
CPMAS	Cross-polarization magic angle spinning
DCM	Dichloromethane
DGA	Diglycolamide
DI	Deionized water
DMF	N,N-dimethylformamide
DoD	Department of Defense
DOE	Department of Energy
DTPA	Diethylenetriaminepentaacetic acid
Dy	Dysprosium
EDS	Energy dispersive spectroscopy
EXAFS	Extended X-ray absorption fine structure
FTIR	Fourier-transform infrared
ICP-MS	Inductively coupled plasma mass spectrometry
LED	Light emitting diode
MCF	Mesoporous carbon fiber
MMS	Magnetic mesoporous silica
Nd	Neodymium
NMR	Nuclear magnetic resonance
PAN	Polyacrylonitrile
PEI	Polyethyleneimine
PMMA	Polymethyl methacrylate
PP	Phosphonate
Pr	Praseodymium
REE	Rare earth element
SEM	Scanning electron microscopy
SRNL	Savannah River National Laboratory
US	United States
WP	Weapons Systems and Platform
XANES	X-ray absorption near-edge structure
XAS	X-ray absorption spectroscopy
XPS	X-ray photoelectron spectroscopy
XRD	X-ray diffraction

Keywords

Citrate-assisted extraction
Dysprosium
Mesoporous carbon
Mesoporous silica
Neodymium
NdFeB magnet
Organic ligand functionalization
Praseodymium
Rare earth elements
Solid-liquid separation
X-ray absorption spectroscopy
X-ray electron spectroscopy

Acknowledgements

The investigators would like to thank Savannah River Ecology Laboratory, University of Georgia, for technical support in batch experiments and associated sample analyses, and Canadian Light Source for technical support with X-ray absorption spectroscopy measurements.

Functionalized Mesoporous Carbon and Silica for Effective Recovery of Rare Earth Elements from Magnet Scrap

1 Abstract

The dependence on international supplies of rare earth elements (REEs) have prompted the US to explore alternative sources and sustainable technologies for domestic REE production. One potential source is the secondary electronic and industrial wastes at the Department of Defense (DoD) complexes and across the US. These hazardous wastes require high costs for the maintenance and remediation, while their high-REE contents offer unique opportunities for REE recovery. However, current hydrometallurgical technologies for REE extraction are energy intensive and costly, with low REE recovery rate and the generation of toxic wastes. Thus, it is beneficial to develop environmentally friendly technologies for REE extraction and processing from the secondary wastes. This project aims to develop novel functionalized mesoporous carbon fiber (MCF) and silica for effective recovery of REEs from end-of-life NdFeB magnet scrap.

Novel MCF and silica materials were synthesized, functionalized with selected organic ligands and characterized. The functional MCF and silica materials were evaluated using batch experiments for the effectiveness of Nd, Pr, and Dy recovery from acidic citrate extraction simulants and real NdFeB powder extraction solutions. The MCF and mesoporous silica after adsorption reaction were also evaluated for the regeneration, reuse and REE harvest. In addition, molecular-level interactions and binding mechanisms between Nd and MCF surface functional ligands were investigated using Nd L_3-edge and C, N and O K-edge synchrotron X-ray absorption spectroscopy (XAS), which will facilitate the design of more robust mesoporous materials.

Biodegradable organic ligands (e.g., citrate) can assist the extraction of Nd and Pr from NdFeB powder at pH 2-3 and significantly reduce the use of mineral acids (e.g., HCl) and the generation of new strong acidic waste. MCF synthesized using PMMA-*b*-PAN block copolymer template was effective at Nd adsorption from DI water and 50 mM citric acid simulant, with Nd binding with MCF as a corner-sharing mode. For real NdFeB extraction, MCF was not effective for Nd and Pr recovery; however, diethylenetriaminepentaacetic acid (DTPA) functionalized MCF significantly improved Nd and Pr recovery rate. Phosphonate (PP)- and polyethyleneimine (PEI) functionalized magnetic mesoporous silica (MMS) exhibited Nd adsorption capacities of 15 mg/g from 50 mM Na citrate and HCl solutions (pH 2.5). The functionalized MMS materials remained effective after four adsorption-desorption cycles. The MMS-PP and MMS-PEI shows significantly improved Nd, Pr and Dy recovery rates from real NdFeB extraction solutions.

The new functional MCF and silica platform technology (**Figure 1**) would bring the following technical benefits: 1) improved selectivity and extraction capacity for REEs, 2) improved stability, life span, and reusability of sorbent materials in acidic media, 3) reduced processing steps and costs for REE recovery, 4) reduced release of toxic wastes and risks to human health and environment, 5) high scalability and robustness of the separation technology. The development and optimization of this technology will ultimately facilitate the domestic recovery of REE from electronic and industrial wastes in environmentally friendly manner, while mitigating the environmental risks of the wastes at DoD complexes and across the US.

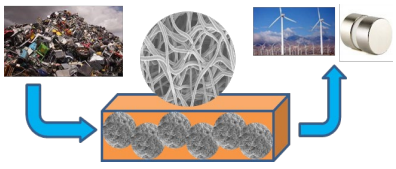

Figure 1. Mesoporous carbon fiber and silica platform technology.

2 Objective

This seed project aimed to develop new functionalized mesoporous carbon fiber (MCF) and silica for effective recovery and separation of rare earth elements (REEs) from the weak acidic extracts of end-of-life NdFeB magnet scrap and to provide a proof-of-concept for the recovery and separation of REEs from other electronic and industrial wastes. The proof-of-concept data need to demonstrate that the MCF and silica of tunable pore size, pore structure and surface functionalities can be synthesized to provide high surface areas and more active sites for high REE adsorption capacity. Furthermore, selected organic ligands can be functionalized into the pore structure to improve REE selectivity of the MCF and silica materials against other competitive cations from complex extraction solutions. NdFeB powder was used as a representative model feedstock to NdFeB magnet scrap to acquire critical proof-of-concept data. The ultimate goal of this research is to design and optimize functional and tunable MCF materials for the recovery and separation of REEs from magnet scrap and other electronic, defensive, and industrial wastes, and meanwhile, for reducing the management risk and cost of the waste streams.

Key **technical questions** to be answered are: 1) how the MCF and silica materials of tunable pore size, pore shape, and surface functionalities can be synthesized and functionalized with novel organic ligands, 2) how the new MCF and silica materials can be utilized for effective recovery and separation of REEs from complex weak acid extracts of NdFeB magnet scrap or other secondary waste streams, and 3) how the MCF and silica materials can be regenerated for reuse and REEs harvest. To address these questions, the following **specific objectives** were achieved: 1) Novel MCF materials of tunable pore size, pore shape, and functionalities were developed using polymethyl methacrylate (PMMA)-polyacrylonitrile (PAN) block copolymers (PMMA-*b*-PAN) template; 2) Diglycolamide (DGA) and diethylenetriaminepentaacetic acid (DTPA) were selected to functionalize onto the MCF using post-synthesis methods, which would effectively recover and potentially separate neodymium (Nd), praseodymium (Pr), and dysprosium (Dy) from the acidic citrate extraction simulants and real acidic extracts of NdFeB powder; 3) Reactivity and molecular binding mechanisms of REEs with surface ligands were investigated using advanced spectroscopic techniques, which will facilitate the molecular design of organic ligands and tunable MCF. In order to reduce material preparation risk and for comparison purpose, polyethyleneimine (PEI) and phosphonate (PP)-functionalized mesoporous silica materials were synthesized and evaluated for Nd adsorption from acidic citrate extraction simulants and for Nd, Pr and Dy recovery from real extraction solutions of NdFeB powder.

While this seed project was focused on the development of innovative MCF and silica materials for effective and selective concentration and separation of REEs from complex waste streams, in order to mitigate the generation of strong acidic waste solutions, citrate ligand-assisted hydrochloric acid extraction was used in dissolving NdFeB powder and provide a REE-containing feeding solution for the REE recovery. Readily biodegradable and less expensive citrate ligand can facilitate REE extraction via both proton and ligand-complexation promoted dissolution processes, with the expected pH values of 2–7 for the extraction solutions, which can greatly reduce the amount of hydrochloric acid, meanwhile, achieve similar or even improved REE extraction rates, and minimize the environmental impacts from the use of traditional strong mineral acids. Thus, this research enables to meet the goals of the SERDP Scope of Need (SON) in exploring new sources for domestic REE production, addressing national resource security issues and reducing hazardous solid/liquid waste streams and their environmental risks.

3 Background

3.1 Problem Statement

Rare earth elements (REEs) are a group of 15 lanthanide elements, scandium (Sc), and yttrium (Y), with similar chemical properties.[1] REEs are critical materials that are widely used in various industries, defense technologies, and medicine. Numerous environmentally sound technologies employ REEs for rechargeable batteries, LEDs, fluorophores, magnetic materials, and lasers.[2,3] Given the increasing global demand for green and sustainable products, REE demand is projected to increase rapidly in the US and globally. Current REE production in the US is very low (26K metric tons in 2019), even though the US possesses ~9% of the global REE resources.[4,5] With potential risks of geopolitical conflicts, future REE supplies in the US might become uncertain and even at risk of disruption. Thus, the US is actively exploring new REE resources to secure future supplies. Conversely, the widespread use of various REE-containing products generates millions of tons of electronic and industrial wastes in the US and globally, including the DoD complex. These secondary solid wastes impose high risks to the environment and ecosystems, and their remediation and safe disposition are highly costly. To address challenges with both REE recovery from waste streams and the management/valorization of electronic wastes, one of DoD and the US's critical material strategies is to develop novel and environmentally friendly technologies to recover REEs from spent catalysts, magnets, electronic wastes, and other secondary waste sources.[6-13]

However, extracting REEs from secondary waste sources is very challenging. Mineral acids are routinely used to extract REEs from wastes,[7] although some studies proposed the use of organic acids, bacteria, or microbially derived organic ligands/acids.[14,15] Both mineral and organic acid based methods generate acidic solutions with variable pH values and typically low concentrations of REEs and high concentrations of impurities (*e.g.*, competing cations Fe^{3+} and Al^{3+}). These characteristics (low pH, low REE content, complex composition) of the extracts from secondary wastes make the recovery and separation of REEs extremely challenging and must be addressed with novel technologies targeting selective REE recovery from secondary wastes. On the other hand, even for the processing of REE mineral ores with high REE contents, technological innovations are still much desired. Traditional hydrometallurgical technologies for the processing of REE ores involve complex multi-step extraction processes. REEs are typically dissolved from the mineral ores using strong mineral acids (*i.e.*, HF, HNO_3, HCl, and H_2SO_4), followed by multi-step solvent extractions to recover and separate REEs.[16] The overall process is tedious and costly, has low REE extraction efficiency, and generates toxic liquid/solid wastes that pose high risks to the environment and ecosystems.[17] Taken together, for the processing and extraction of REEs from both secondary wastes and mineral ores, **one critical challenge for downstream processing** is the recovery of REEs from acidic extracts and the selective separation of REEs from other cations. Any promising new processing methods/materials must also be environmentally friendly, stable under variable acidic conditions, and flexible to accommodate different solution compositions.

3.2 The State of the Science

3.2.1 REE Recovery from Waste Sources

In recent years, coal ashes,[18,19] phosphogypsum,[20] electronic wastes, and spent magnets[21-23] have been considered as promising REE resources. Mineralogy and geochemistry of REEs in these alternative REE resources have been studied in order to develop proper pretreatment and extraction strategies. For example, a recent study from Co-PI Tang's group identified a range of heavier REE-bearing phases in coal ashes, such as REE phosphates, apatite, and zircon, suggesting that density separation might be used for pre-enrichment of REEs.[24] After pretreatment, mineral acids (*i.e.*, HNO_3, HCl, and H_2SO_4) are the most commonly used agents for extracting REEs from waste sources such as coal ash.[25,26] After the extraction step, REEs can be further recovered, concentrated, and separated from the acidic solutions using various conventional separation processes.[27-31] In order to minimize environmental impacts during REE extraction from waste sources, research has been directed to the utilization of organic acids[32,33] or biological methods,[34-37] and some studies have shown REE extraction efficiency comparable to mineral acids. For example, Biolixiviant, consisting of spent medium containing organic acids from the growth of the bacterium *Gluconobacter oxydans* on glucose, was more efficient than gluconic acid and H_3PO_4 in REE extraction from synthetic REE-doped phosphogypsum.[38]

Ionic liquids[39-45] and membrane solvent extraction[23,29] were recently proposed as alternatives to conventional solvent extraction. These methods demonstrated some advantages, such as negligible vapor pressure and non-flammability, and decreased non-aqueous solvent use, but still have several drawbacks. For example, the synthesis of ionic liquids is currently costly, and the high viscosity of ionic liquids slows down mass transport in large-scale processes. The stripping of REEs from ionic liquids requires another solvent because the contact of ionic liquids and solvents may result in cross-contamination.[40] Considering all the advantages and drawbacks of current processes for REE extraction from acidic media, designing alternative recovery and separation technologies is of great urgency and importance.

3.2.2 REE Recovery from NdFeB Magnet Scrap

NdFeB magnets contain 20–25% Nd and low concentrations of Dy and Pr and exhibit superior magnetic and mechanical properties. They are widely used in various industries and defense technologies, such as in electronics (*e.g.*, hard disks, mobile phones, electronic displays), automotive, medical devices, next generation wind turbines, and advanced military weapons systems (*e.g.*, sensors). As a result, large amounts of NdFeB magnet scrap are generated and mostly lost to landfills. The extraction of REEs from NdFeB magnet scrap has been attempted using traditional mineral or organic acid leaching[32,46] followed by solvent extraction,[47-50] ion liquid extraction,[46] membrane assisted solvent extraction,[23] or two-zone ligand-assisted displacement chromatography[51]. Selective chlorination of Nd using NH_4Cl[52], selective extraction of Nd using molten chlorides,[53] selective leaching of Nd using electrochemical method[54] and guanidine hydrochloride−lactic acid combined deep eutectic solvents[55] have also been investigated recently. However, hydrometallurgical and ion liquid methods suffer similar drawbacks as described above. The recently reported methods for selective Nd extraction are only evaluated at lab scale. More effective and environmentally friendly technologies for extraction of Nd, Dy, and Pr from NdFeB magnet scrap are highly desired.

3.2.3 Mesoporous Materials for REE Recovery

Solid-liquid extraction can potentially overcome the shortcomings (*i.e.*, high cost, low REE recovery rate, and toxic liquid/solid wastes) associated with liquid-liquid extraction of REEs from acidic media, especially with the development of novel advanced materials. Mesoporous silica has large and tunable pores by size and geometry. The pores can be readily functionalized with organic ligands,[56] which can greatly enhance the effective and selective sequestration of various metals from aqueous media.[57] Extensive research work has been conducted on the synthesis, functionalization, and applications of mesoporous silica, including the recovery and separation of REEs.[58-60] For example, maleic anhydride,[61] titanium alkylphosphate,[62] 1-(2-Pyridylazo) 2-naphthol and acetylacetone,[63] tetradentate phenylenedioxy diamide,[64] phosphonoacetic acid, N,N-bisphosphono(methyl)glycine, and diethylenetriaminepentaacetic dianhydride[65] have been functionalized on mesoporous silica. These systems demonstrated capabilities of improving the efficacy for extracting REEs from acidic to circumneutral solutions. However, only limited selectivity for light and heavy REEs can be realized, and the nature of metal binding and the correlation between ligand functionalization density and observed separation factors are not well understood.

Mesoporous carbon materials are less studied for surface functionalization and REE separation. A recent research reported that synthetic mesoporous carbon (*i.e.*, CMK-8) can be oxidized with hydrogen peroxide to increase the quantity of oxygen groups on the carbon surface and subsequentially functionalized by appending diglycolamide (DGA)-based ligands on oxygenated CMK-8 surfaces.[66] The derived new carbon materials showed high stability under acidic conditions as well as improved extraction performances for REE recovery in terms of both selectivity and adsorption capacity.[66] However, ligand grafting and lanthanide binding on DGA-functionalized materials appears incomplete, since the 2:1 ratio of N:Cl in reported energy dispersive spectroscopy (EDS) data indicates only one arm of DGA being appended to the surfaces. In addition, bis-(2-ethylhexyl)phosphoric acid physisorbed on large pores of mesoporous carbon has been evaluated as a chromatographic material for a small-scale separation of Nd^{3+} and Eu^{3+}.[67]

3.3 Proposed Technology and Its Benefits

To address the challenges for REE extraction from waste sources, this seed project aimed to develop novel functionalized **mesoporous carbon fiber (MCF)** and acquire proof-of-concept data which can demonstrate the novel MCF materials' effectiveness for selective recovery of REEs from acidic citrate extraction simulants and real acidic extracts of NdFeB powder as a model feedstock to its magnet scrap. In order to enable the rational design of functionalized MCF for efficient and selective REE extraction, this project would also delineate clear structure-function relationships for the selective binding of REEs in mesopores of MCFs that are functionalized with novel organic ligands. More specifically, citrated assisted dissolution methods were developed for extraction of REEs from NdFeB powder. Novel MCF materials were designed and synthesized using polymethyl methacrylate-polyacrylonitrile block copolymer (PAN-*b*-PMMA) template. After thorough characterization, the MCF materials were functionalized with novel organic ligands, diglycolamide (DGA) and diethylenetriaminepentaacetic acid (DTPA), using post-synthetic methods. Batch experiments were conducted to evaluate the effectiveness and reactivity of the functionalized MCFs for REE binding, concentration, and release from acidic citrate extraction simulants and real acidic extracts of NdFeB powder. Neodymium L_3-edge and C, N and O K-edge synchrotron X-ray spectroscopy (XAS) were collected to investigate Nd-ligand

interaction and reveal structure-function relationship. In order to reduce material preparation risk and for comparison purpose, polyethyleneimine (PEI)-and phosphonate (PP)-functionalized mesoporous silica materials were also synthesized and evaluated for Nd adsorption from acidic citrate extraction simulants and for Nd, Pr and Dy recovery from real extraction solutions of NdFeB powder.

This seed project established a proof-of-concept on the design and application of MCF- and silica based molecular materials for REE extraction from NdFeB powder. The proof-of concept data demonstrates that these novel materials are stable under acidic conditions, highly tunable to accommodate variable feedstock and composition, selective toward REEs against other impurities, and environmentally friendly to address the issues with both REE processing and waste management. Moving forward, the successful development and optimization of this material group and conceptual approach will enable: 1) effective recovery and separation of REEs from different electronic/industrial wastes, 2) mitigation of the generation of toxic wastes during recovery process, 3) reduction in management risk and disposition costs for secondary electronic wastes. Although this SEED project only examines NdFeB powder as a model feedstock for a proof-of-concept demonstration, with reduced risks due to the acquired seed data, the developed technology will be applicable to REE extraction from NdFeb magnet scarp and other electronic / industrial waste streams. The future research will incorporate high throughput computation and machine learning to further optimize the rational design of molecular MCF and mesoporous silica materials and operation processing for REE extraction, not only from magnet scrap but also other electronic and industrial wastes that are widely present at the DoD complex and the US.

4 Materials and Methods

4.1 Citrated assisted extraction of REEs from NdFeB Powder

A commercial NdFeB powder was acquired from Alibaba and used to represent NdFeB magnet scrap for this proof-of-concept study. Its chemical compositions were analyzed by inductively coupled plasma mass spectrometry (ICP-MS) following total digestion (**Table A1).** Major REEs are Nd 22.36 wt%, Pr 3.48 wt%, Ce 0.39 wt%, La 0.25 wt%, and Dy 39 ppm. Other major elements are Fe 69.85 wt%, B 1.45 wt%, Co 1.00 wt% and Al 0.33 wt%.

A green extraction method was developed using organic ligand (citrate) and diluted HCl solution to extract REEs from the NdFeB powder. A matrix of solution chemistry was tested and optimized to achieve maximal extraction efficiency. Tested parameters include organic acid type/concentration, pH, extraction time, and reaction cycles. NdFeB powders were added to a solution containing varied concentrations of sodium citrate (e.g., 1–100 mM) at pH 2–7 and allow to react for single or multiple cycles of 0–24 h under agitation. After extraction, solid and liquid phases were separated using vacuum filtration. Metal concentrations in the filtrate were measured by ICP-MS.

4.2 Synthesis of MCFs

In order to rationally design MCF materials for the selective recovery and separation of REEs, the essential elements that must be controlled precisely are the pore size (2–50 nm), shape (cylindrical, gyroid, and perforated lamellae), and surface functionalities. There are many methods to prepare mesoporous carbon using different templates.[68,69] The final pore sizes of mesoporous

carbon can be controlled by selecting appropriate templates, carbon precursor/template ratio, carbonization temperature, and synthesis methods.[66,68] A new synthetic method to prepare MCFs using PMMA-*b*-PAN block polymer template was developed.[70-73]

In this project, PMMA-*b*-PAN was synthesized by reversible addition−fragmentation chain transfer polymerization (**Figure 2**). First, methyl methacrylate (35.0 mL, 309 mmol), cumyl dithiobenzoate (CDB, 84.3 mg, 0.309 mmol), and 2,2'-azobis(2-methylpropionitrile) (AIBN, 25.4 mg, 0.155 mmol) were dissolved in benzene (51.6 mL) in a 250 mL Schlenk flask. The mixture was subjected to three freeze−pump−thaw cycles to remove the dissolved oxygen. Then, the flask was put in an oil bath maintained at 60 °C for 24 h with continuous stirring to synthesize PMMA macrochain transfer agents (CTAs). The resulting PMMA macro-CTAs were precipitated in methanol and filtered. The resulting polymer was dried at room temperature in a fume hood overnight. The purified PMMA macro-CTA was used to synthesize PMMA-*b*-PAN block copolymers. To do so, PMMA macro-CTA (5.1 g, 108 μmol), AN (26.0 mL, 433 mmol), AIBN (4.4 mg, 27 μmol), and dimethyl sulfoxide (DMSO, 72.2 mL) were mixed in a 250 mL Schlenk flask. The mixture was degassed by three freeze−pump−thaw cycles and then heated in an oil bath at 65 °C for 24 h with continuous stirring. The PMMA-*b*-PAN block copolymer was purified following the same steps as PMMA macro-CTAs. The as-synthesized PMMA macro-CTA and PMMA-*b*-PAN were characterized by size exclusion chromatography (**Figure A1**). The average molecular weight of PMMA is 47 kDa and the dispersity is 1.03. The number average molecular weight of PMMA-*b*-PAN is 115 kDa and the dispersity is 1.13. The structure of PMMA macro-CTA and PMMA-*b*-PAN is characterized by ^{1}H NMR (**Figure A2**).

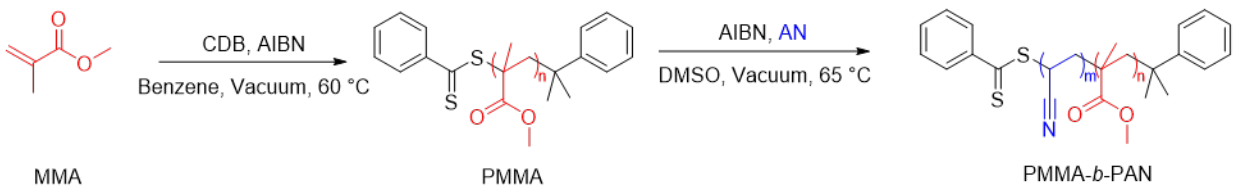

Figure 2. Synthesis route of PMMA-*b*-PAN block copolymer.

As shown in **Figure 3**, MCF materials were prepared by electrospinning, oxidation, and pyrolysis. PMMA-*b*-PAN block polymers were dissolved in dimethylformamide at a concentration of 16 wt%. The solution was stirred under a mild heating condition to fully dissolve the polymers. Then the solution was electrospun into polymer fiber mats using a readily electrospinning station in the Liu laboratory. The block copolymer fibers were collected in an in-house-built rotary Al drum. Oxidization and pyrolysis of the fibers were conducted in a tube furnace at elevated temperatures. The fiber mats were first oxidized by heating in the air from room temperature to 280 °C (heating rate, 1 °C/min) and isothermally stabilized at 280 °C for 12 h. After oxidation, the fiber mats were heated again at 1000 °C to completely pyrolyze the polymer into MCFs. The prepared MCFs were characterized by powder X-ray diffraction (XRD), scanning electron microscopy coupled with energy dispersive spectroscopy (SEM-EDS), Fourier transform infrared (FTIR) spectroscopy, as well as surface area, porosity and pore diameter measurements using N_2 adsorption.

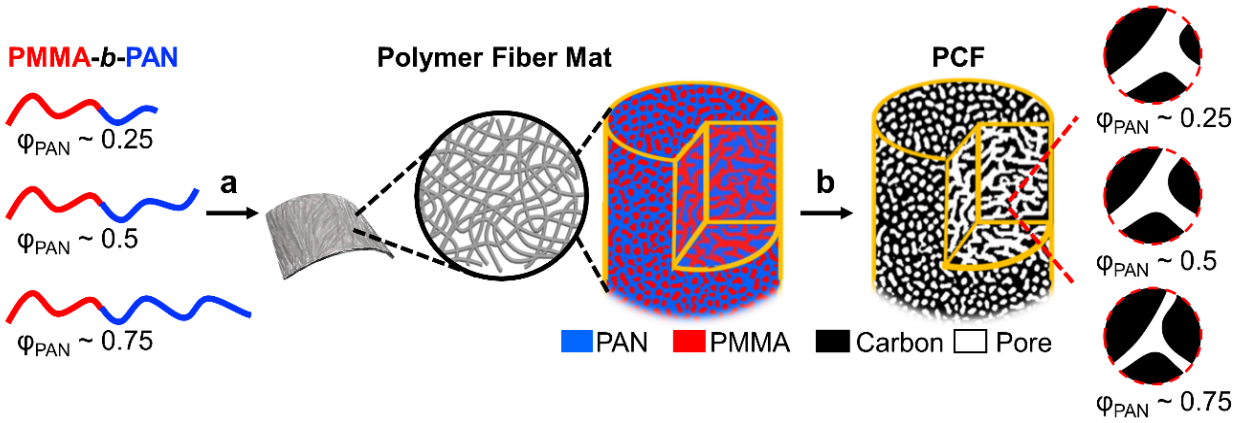

Figure 3. (a) PMMA-*b*-PAN of varying molecular weights and compositions are electrospun into a fiber mat. (b) After phase-separation of PAN (blue) and PMMA (red), polymer fibers are oxidized and carbonized into porous carbon fibers. The block copolymer composition controls the pore size, surface area, and ion diffusion properties.

4.3 Organic Ligand Functionalization of MCFs

After detailed characterization, the MCFs were functionalized with diglycolamide (DGA) and diethylenetriaminepentaacetic acid (DTPA) (**Figure A3**). These two functional ligands are stable at pH 1–2 and allow for the modulation of donor numbers and relative chain length.[74] Two carbonyl oxygen and an ether oxygen on DGA are involved in the chelate interactions with trivalent metal ions to form a two-membered ring complex, while DTPA is an octadentate aminopolycarboxylate complexing agent, both ligands are expected to be very effective for binding trivalent REEs.

4.3.1 Synthesis of Ligands with APTS

Two step approach was used for DGA and DTPA functionalization onto MCFs. First, DGA or DTPA ligand was coupled with (3-Aminopropyl)triethoxysilane (APTS). After oxidation of MCFs, the ligands were then functionalized onto MCFs through APTS coupling agent.

Figure 4 shows the synthesis scheme of APTS-DGA. First, diglycolic acid (0.47 g) was dissolved in dichloromethane (DCM, 30 mL). Then 5 drops of N,N-dimethylformamide (DMF) and oxalyl chloride (0.75 mL) were added to the solution at 0 °C with continuous N_2 flow. The mixture was stirred at room temperature under an N_2 atmosphere for one day. After the reaction, DCM was removed by rotary evaporation. The product was characterized by ^{1}H NMR (**Figure A4**). The peak at 7.25 ppm is the solvent deuterated chloroform. The peaks at 5.3 ppm and 4.6 ppm are diglycolyl chloride and diglycolic acid respectively. The ratio of the peak integration of diglycolyl chloride to diglycolic acid is 1:0.03, which indicates most of the diglycolic acid was converted to diglycolyl chloride. Second, diglycolyl chloride was dissolved in 20 mL of DCM. Then 2 mL of ATPS and 0.2 mL of triethylamine (Et_3N) were added to the solution at 0 °C under N_2 flow. The mixture was stirred under N_2 atmosphere at room temperature for one day. After the reaction, water was added to the mixture. Acetone was then added to the water layer to precipitate

the product. The product was filtered and dried at 100 °C. The structure of the product was characterized by FTIR (**See Section 5.3**).

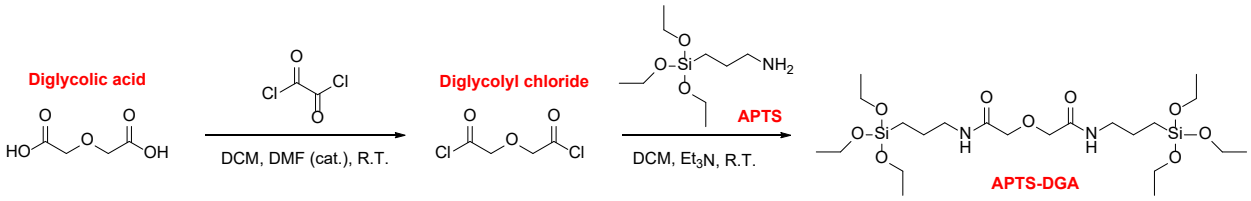

Figure 4. Synthesis scheme of APTS-DGA.

Figure 5 shows the synthesis scheme of ATPS-DTPA. First, 0.98 g of DTPA and 2.03 g hydroxybenzotriazole were dissolved in 10 mL of DMF. Then, 1.47 mL of APTS, 2.88 g N-(3-Dimethylaminopropyl)-N′-ethylcarbodiimide hydrochloride in 10 mL DMF solution, and 4.36 mL Et_3N were added to the mixture at 0 °C with continuous N_2 flow. The mixture was stirred at room temperature under an N_2 atmosphere for one day. After the reaction, water was added to the mixture. The product was precipitated by acetone from the water layer and dried at 100 °C. The structure of the product was characterized by FTIR (**See Section 5.3**).

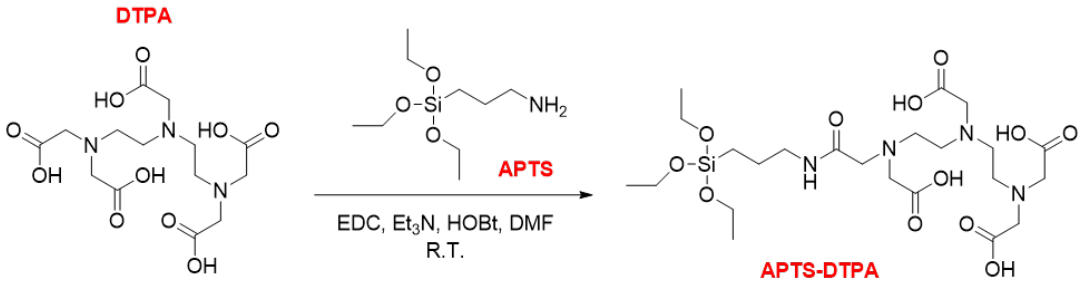

Figure 5. Synthesis scheme of APTS-DTPA.

4.3.2 Oxidation of MCF

MCF (1 g) was mixed with 30 mL of concentrated H_2SO_4 and 10 mL of concentrated HNO_3. The mixture was heated at 75 °C for 12 h without stirring. After the reaction, the mixture was diluted with 200 mL of water and the oxidized MCF was separated by centrifugation. Then the product was washed with water 3 times to remove the remaining acid and dried at 100 °C overnight. The oxidized MCF was characterized by FTIR (**See Section 5.3**).

4.3.3. Ligand Functionalization to MCF

For DGA and DTPA ligand functionalization to MCF, oxidized MCF (1 g) and 0.5 g of APTS-DGA or APTS-DTPA were mixed in 30 mL of toluene. 0.5 mL of Et_3N was added to the mixture under N_2 flow. The mixture was refluxed for one day. After the reaction, toluene was removed by rotary evaporation. Unattached DGA ligands were removed by DCM, and unattached DTPA ligands were removed by water. The products were dried at 100 °C overnight. The structure of the products was characterized by FTIR (**See Section 5.3**).

4.4 Synthesis of Functionalized Magnetic Mesoporous Silica

As shown in **Figure 6**, two steps were used in the synthesis of functionalized magnetic mesoporous silica. In Step 1 to prepare magnetic mesoporous silica (MMS), Fe_3O_4 was first synthesized using a previous reported method.[75] 4.8 g ferric chloride and 2.0 g ferrous chloride were dissolved in 30 mL deionized water, which were allowed to stir under nitrogen atmosphere at the temperature of 90 °C. 20 mL NH_4OH solution was added to precipitate Fe_3O_4, and the suspension was aged for 2.5 h, then filtered and washed with deionized water and dried at 100 ºC. Magnetic mesoporous silica (MMS) was synthesized using an approach previously described for mesoporous silica (MCM-41) synthesis,[76,77] in the presence of Fe_3O_4 nanoparticles. Typically, 1 g cetyltrimethylammonium bromide (CTAB), 3.5 mL 2M NaOH, and 500 mL water were mixed with 300 mg Fe_3O_4 and sonicated, which was heated at 80 °C and then tetraethoxysilane was added. The reaction mixture was aged for 2 h and then filtered, washed with deionized water and methanol, and dried at 120 °C overnight. The CTAB template was removed by calcining the product at 600 °C in flowing compressed air for 6 h to obtain MMS.

In Step 2 to prepare functionalized MMS, for functionalization with phosphate (PP) group, 1 g calcined MMS was refluxed with 3-(trihydroxysilyl)propyl methylphosphonate (4 mmol) in 1,4-dioxane at 100 °C for 4 h. The reaction mixture was filtered, washed with 1:1 mixture of diethyl ether and dichloromethane, and dried at 100 °C overnight to obtain phosphonate-functionalized MMS (MMS-PP).[78] The PEI-functionalized MMS was prepared by a wet impregnation method. The desired amount of PEI was dissolved in 8 g of methanol under stirring for about 15 min, after which 2 g of calcined MMS was added to the solution. The resultant slurry was continuously stirred for about 30 min, and then dried at 70 °C for 16 h under 700 mmHg vacuum to obtain PEI-functionalized MMS (MMS-PEI).[79]

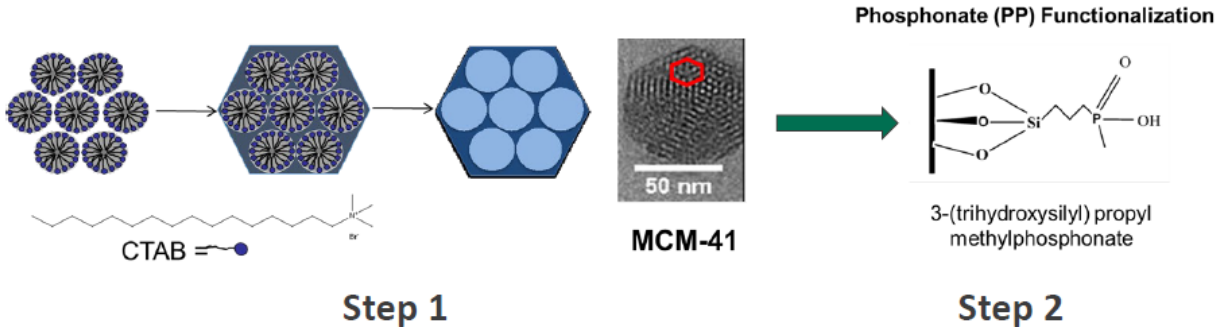

Figure 6. Synthesis scheme of functionalized magnetic mesoporous silica (MMS).

4.5 Batch Experiments

Batch adsorption experiments were conducted to evaluate the efficiency and selectivity of the MCF and silica materials for recovering Nd, Dy, and Pr from acidic extraction simulants or real extraction solutions of NdFeB powder. Batch Nd^{3+} adsorption experiments were conducted at an initial Nd concentration of 5×10^{-4} M in deionized (DI) water and 50 mM sodium citrate extraction simulant (its pH was adjusted to ~2.3 using 2 M HCl solution) under ambient condition. For each set of experiments, a solid-free control was included as the initial Nd concentration for

recovery rate and adsorption quantity calculation. Typically, 0.025 gram of sorbent materials and 2.5 mL solution were added to 15 mL polypropylene centrifuge tubes. Neodymium nitrate hexahydrate ($Nd(NO_3)_3 \bullet 6H_2O$, Alfa Aesar) was used to make the Nd stock solution of 5×10^{-2} M. After spiking with 0.025 mL of the Nd stock solution, the suspensions were equilibrated on a reciprocating shaker for 1 day if not specified. After equilibration, each suspension was centrifuged at 10,000 rpm for 10 minutes and filtered using 0.2 μm pore size polyethersulfone membrane filter. After pH measurement, a certain amount of the filtrate was acidified with 2% HNO_3 in an appropriate dilution ratio and analyzed for Nd by ICP-MS (NexION 300X, Perkin Elmer, Inc.). The ICP-MS analysis uncertainty was within ±5%. The Nd recovery rate and the mass of Nd sorbed onto the sorbent (qe, mg/g) were calculated using equations 1 and 2, respectively:

$$Recovery\ rate = \frac{C_0 - C_e}{C_0} \times 100 \quad (1)$$

$$q_e = \frac{(C_0 - C_e) \times V}{M} \quad (2)$$

where C_0 (mg/L) is the initial Nd concentration in the control samples, Ce (mg/L) is Nd concentration in the solution at equilibrium, V is the volume of the solution (mL) and M is the mass of the sorbent (g).

In addition, batch experiments for obtaining the adsorption isotherm curves were conducted at initial Nd concentration ranged from 1×10^{-4} M (14.4 ppm) to 5×10^{-3} M (721 ppm), 0.025 gram of the solid and 2.5 mL DI water or 50 mM sodium citrate and HCl acid simulant. For the adsorption/desorption cycle evaluation, the sorption experiments were conducted using 50 mM sodium citrate in pH 2.3 simulant with an initial Nd concentration of 5×10^{-4} M, solid/liquid ratio of 10 g/L, and reaction time of 30 minutes, while the Nd desorption experiment was conducted using 1 M HCl solution and 30 minutes. For real extraction solutions of NdFeB powder, the batch experiments were conducted with 0.025 g sorbent in contact with the extraction solution (solid/liquid ratio of 10 g/L) for 24 hours.

4.6 Characterization Methods of Materials

4.6.1 N_2 adsorption-Desorption Measurements

To characterize the surface area and pore size distribution of the MCF materials, N_2 physisorption was conducted by a 3Flex pore analyzer (Micromeritics Instrument Corp.) at 77 K. The surface area was calculated by Brunauer−Emmett−Teller (BET) theory, and the pore size distribution was determined by nonlocal density functional theory.

4.6.2 Fourier Transform Infrared (FTIR) Spectroscopy

Fourier Transform Infrared (FTIR) spectra were measured between 4000 and 400 cm^{-1} on a Nicolet iS 5 FTIR Spectrometer to characterize the surface functionalization of MCF.

4.6.3 Scanning Electron Microscopy-Energy Dispersion spectroscopy (SEM-EDS)

The synthesized MCF material was characterized using field-emission scanning electron microscope (SEM, LEO 1550). The SEM images were collected using at an accelerating voltage of 2 kV and a working distance of ~3 mm.

4.6.4 X-ray Photoelectron Spectroscopy (XPS)

X-ray photoelectron spectroscopy (XPS) spectra were collected on a PHI Quantera SXM-03 Scanning XPS Microprobe.

4.6.5 Synchrotron X-Ray Absorption Spectroscopy (XAS)

Neodymium L_3-edge X-ray absorption near-edge structure (XANES) and extended X-ray fine structure (EXAFS) spectra of air-dried solid samples were collected using the Canadian Light Source (CLS) Biological X-ray Absorption Spectroscopy (BioXAS, 07ID-2) beamline (Saskatoon, SK, Canada). The BioXAS beamline was optimized for high sensitivity and high-resolution hard X-Ray absorption spectroscopy experiments. Double crystal Si (220) monochromator was used to scan the photon energy in the vicinity of Nd L_3 absorption edge at 6208 eV. Rh-coated toroidal mirrors performed the rejection of 2nd and higher harmonics and moderate beam focusing down to 0.6×2 mm^2 in the sample position with total flux in the order of 1012 photons/s. The experiment was carried out in the energy dispersive fluorescent mode, where the characteristic X-Ray fluorescence from Nd was collected by a Canberra 32-element Ge detector and the incident by N_2-filled ionization chamber. The CLS storage ring was operated at 140–200 mA during the measurements.

All the collected spectra were processed and analyzed using the IFEFFIT software package including Athena and Artemis.[80] Data from multiple scans were processed using Athena by aligning and merging the spectra followed by background subtraction using the AUTOBK algorithm. Neodymium L_3-edge EXAFS data analysis was conducted on the merged and normalized spectra using Artemis.[80] Theoretical models were constructed with the program FEFF7. Bastnasite ($Ce(CO_3)F$) was used as a reference structural model,[81] but Ce was substituted by Nd. Fits to the Nd L_3-edge EXAFS data were made in R space (R from 1 to 3.5 Å) and obtained by taking the Fourier transform (FT) of $\chi(k)$ (k from 2 to 9.6) with a k weighting of 2.

Carbon, nitrogen and oxygen K-edge and Nd M-edge XANES measurements were taken at the CLS High Resolution Spherical Grating Monochromator beamline (11ID-1) in the KB micro-focused (ca. 10 × 50 μm) XAS end-station.[82] To do so, ~1 mg of MCF sample was suspended in 1 mL deionized water, then 1-2 μL of the suspension aliquot was deposited onto a clean Au-coated Si wafer, and the MCF sample was electrostatically adhered to the wafer by drying.[83] Carbon and nitrogen K-edge XANES data of the MCF samples were collected via partial fluorescence yield using a custom-built silicon drift detector (SDD) array. The SDD system was used without pile-up rejection and with the linearity of response controlled by optimization of incident flux via an automated aperture. Individual spectrum was collected at photon energy for C K-edge from 270 to 320 eV, N K-edge from 380-440 eV, O K-edge from 520-570 eV, and Nd M_3-edge from 970-1015 eV using 60 second slew scan to limit radiative dose on the samples. The XANES spectra reported are from the average of 30 spectra, with each spectrum measured at previously unexposed sample positions. The intensity of the incident flux was monitored to permit normalization of the acquired spectra and recorded asynchronously using the SDD-discriminated scattering signal reflected from a clean Au-coated Si wafer.[83] The collected XANES data were

normalized using the software of Athena against the I_0 collected from blank sample holder scattering. The C K-edge data were also calibrated in energy using the primary C 1s→π^* peak of citric acid that was measured at 290.68 eV during our experiments, but reported at 288.7 eV in literature.[84]

5 Results and Discussion

5.1 Citrate Ligand Assisted Extraction of REEs from NdFeB Powder

Batch experiments were conducted to evaluate the extraction efficiency of REEs (Nd, Pr, Ce, La, and Gd) and non-REE major elements (Al and Fe) from NdFeB powders. The studied parameters include reaction time (4–12 h), pH (1–2), citrate concentration (10–500 mM) at a liquid-to-solid ratio of 200 mL/g. The extraction efficiency of all elements at 12 hours almost doubled of that at 4 hours (**Figure 7a**), thus all subsequent experiments were conducted with a reaction time of 12 hours. As shown in **Figure 7b**, the overall extraction efficiency at pH 1 and 2 are not significantly different and both higher than 90%. Increasing citrate concentration from 10 to 100 mM significantly enhanced REE extraction efficiency from ~15% to >90% (**Figure 7c**), but further increase from 100 to 500 mM citrate resulted in negligible improvement (**Figure 7d**). Compared to traditional extraction methods, citrate as a biodegradable organic ligand facilitated REE extraction, while significantly reducing the amount of mineral acid usage and liquid waste.

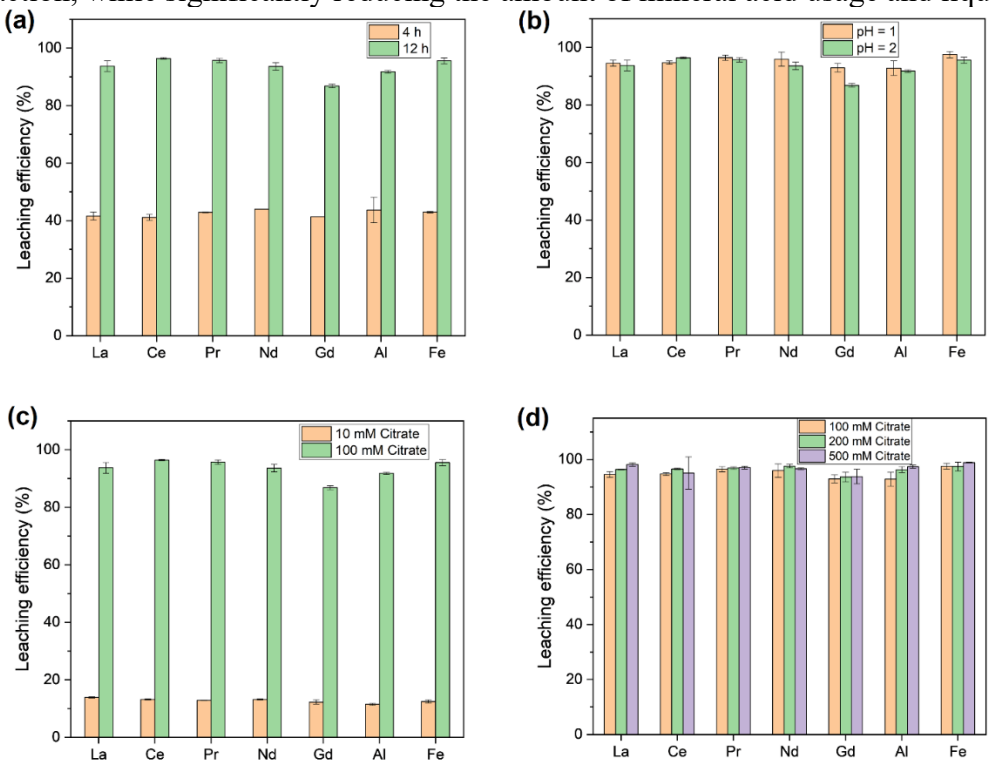

Figure 7. Extraction efficiency of REEs (La, Ce, Pr, Nd, and Gd) and non-REE major elements (Al and Fe) from NdFeB powders under varied conditions: (a) reaction time of 4 or 12 hours (100 mM citrate, pH 2), (b) pH 1 or 2 (100 mM citrate, 12 h), and (c-d) citrate concentration of 10, 100, 200, or 500 mM (pH 2, 12 h). All experiments were conducted with a liquid-to-solid ratio of 200 mL/g and rotation speed 200 rpm.

The leaching efficiency of REEs and other metals from NdFeB magnet at pH 2 and 3 were also studied (**Figure 8a**). Increasing the initial pH from 2 to 3 did not significantly compromise the leaching efficiency of REEs. Notably, high leaching efficiency of Nd, Pr, Sm, Gd, Tb, and Dy (~80–90%) was observed, whereas that of La, Ce, Ho, and Er was between 20–55%. On the other hand, the leaching efficiency of other metals roughly ranged from 20% to 80% (**Figure 8b**). Considering the dominant presence of Nd, Pr, Ce, and La as the major REEs in the magnet materials (Nd 22.36 wt%, Pr 3.48 wt%, Ce 0.39 wt%, La 0.25 wt%, Dy 39 ppm), this represents a high REE extraction efficiency at pH 3, which significantly reduces the usage of mineral acids and generation of hazardous acidic wastes.

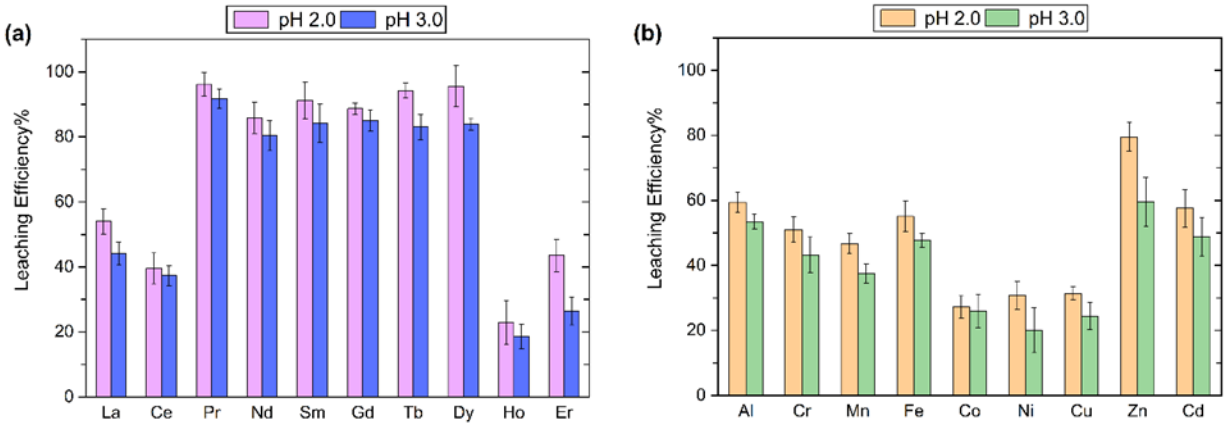

Figure 8. Leaching efficiency of **(a)** REEs and **(b)** other metals from NdFeB magnet at pH 2 and 3 (50 mM citrate, liquid-to-solid ratio: 200 mL/g, 240 rpm, 4 h).

As shown in **Figure 8b**, the citrate extraction solution also contains other metal ions such as Fe and Al. In order to separate REEs from other metals in the solution, 10 mM Ca^{2+} and 20 mM oxalate were added to induce the coprecipitation of a Ca/REE-oxalate phase and separation of Ca/REE from other metal cations. The coprecipitation efficiency represents the fraction of metals that are removed from the solution by calcium oxalate. Overall, this coprecipitation step effectively removed over 70% of REEs into the Ca/REE-oxalate solid phase, while >90% of non-REEs remained in the liquid phase (**Figure 9a and 9b**). The slightly lower coprecipitation efficiency of Nd compared to other REEs could be ascribed to its considerably higher concentration in citrate leachate, which requires further optimization of Ca and/or oxalate concentrations. Varying the solution pH at 2.0 and 3.0 showed no significant impacts on the coprecipitation efficiency. Thus, oxalate precipitation can effectively separate REEs from other metals, including trace amount of divalent metal cations and abundant Fe and Al, and produce a solid phase with high REE content and purity for downstream processing.

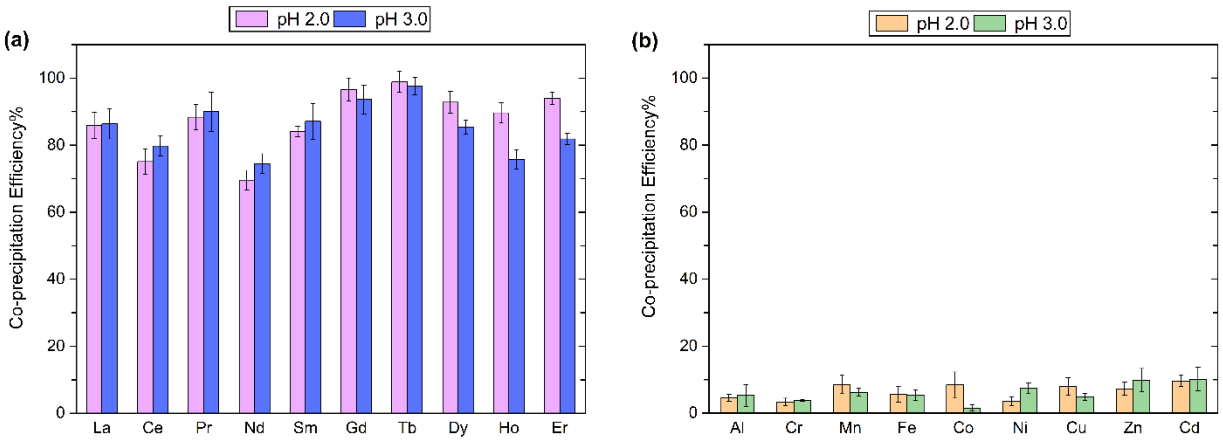

Figure 9. Coprecipitation efficiency of **(a)** REEs and **(b)** other metals by calcium oxalate at pH 2.0 and 3.0 (10 mM Ca^{2+}, 20 mM oxalate, 30 min).

5.2 MCF Materials for REE Recovery

5.2.1 Characterization of MCFs

The original MCF material was characterized using SEM and N_2 adsorption-desorption measurement. The SEM images of the MCF material under different amplifications are shown in **Figure 10**, which shows the carbon fibers with various mesopores developed on the surface and in the cross section of MCF (**Figure 10**).

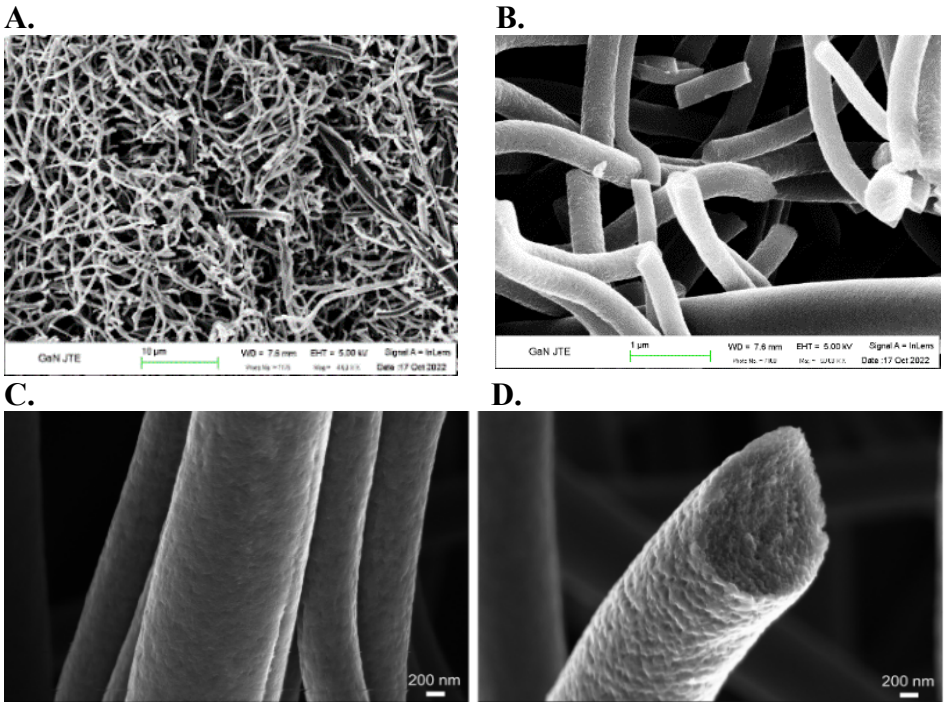

Figure 10. SEM images of MCF synthesized using block copolymer template.

The N_2 adsorption-desorption isotherm of MCF material is shown in **Figure 11A**, which was type IV isotherm and the hysteresis of N_2 isotherm at $0.6 < p/p0 < 0.9$ revealed the presence of mesopores in MCF. The N_2-derived surface area of MCF was 540 m^2/g. The mesopore size distribution of MCF determined by N_2 adsorption displayed a unimodal peak centered at 10.9 nm (**Figure 11B**).

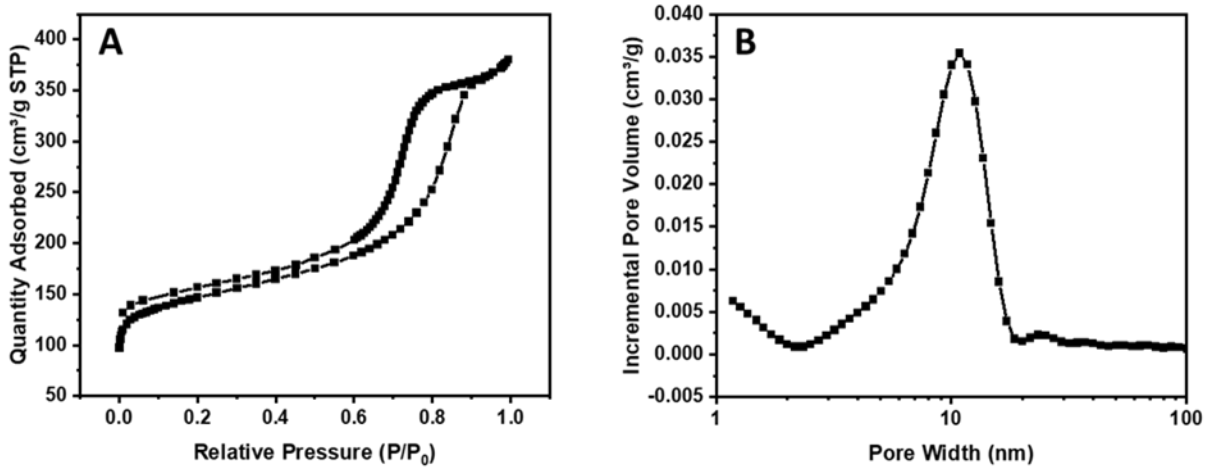

Figure 11. (A) N_2-physisorption isotherms and (B) mesopore size distribution of MCF.

5.2.2 MCF for Nd Adsorption from Extraction Simulants

The Nd adsorption isotherm curves of MCF materials from DI water at the equilibrium pH of ~5.5 and 50 mM citric acid simulant at the equilibrium pH of ~2.3 were obtained based on the batch adsorption experiments and are shown in **Figure 12**, where the labels were the MCF sample numbers. We attempted to fit Nd isotherm data for the MCF material from the two simulant systems to both the Langmuir and Freundlich models, but neither model produces satisfactory results with R^2 values of < 0.90. However, the maximum adsorption capacity of the MCF material can be estimated from the Nd adsorption isotherm curves to be ~20 mg/g from DI waster and ~10 mg/g from the 50 mM citric acid simulant.

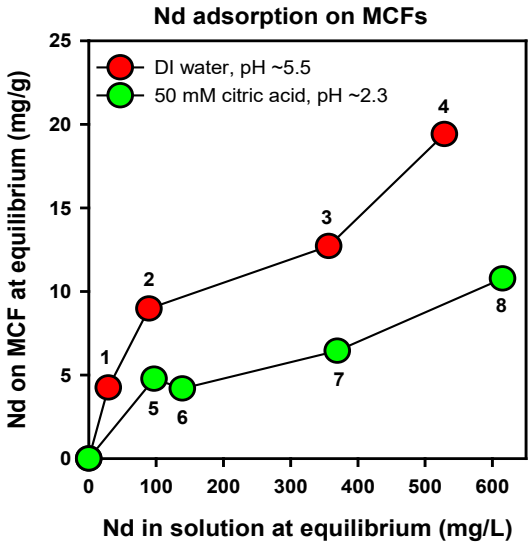

Figure 12. Nd adsorption isotherms onto MCFs (Time: 24 hours, solid/liquid ratio: 10 g/L).

5.2.3 Characterization of MCF after Nd adsorption

The MCF material after Nd adsorption from DI and 50 mM citric acid simulant were characterized using SEM, FTIR and XPS spectroscopy. The SEM images of the MCF after Nd adsorption are shown in **Figure 13A** and **13B**, which indicated that the MCF was stable in terms of its morphology, fiber texture, and pore structure. The FTIR spectrum of the MCF after Nd adsorption (MCF-4) is shown in **Figure 13C**, in comparison with the FTIR spectrum of original MCF. There was a prominent peak at ~1700 cm^{-1} in the spectrum of original MCF and it is attributed to the C=O stretching, but this peak decreased in its intensity to near zero in the spectrum of the MCF after Nd adsorption. These results may indicate that the carboxylic C=O was broken down after Nd adsorption and Nd was bound with the surface C-O groups. The XPS spectrum of the MCF after Nd adsorption (MCF-4) is shown in **Figure 13D**, in comparison with the FTIR spectrum of original MCF. The XPS spectra of MCF before and after Nd adsorption were similar, primarily consisting of C, N and O. The Nd $3d_{3/2}$ (1003.3 eV) and $3d_{5/2}$ (980.4 eV) peaks in the XPS spectrum of MCF-4 after Nd adsorption were not prominent, probably overlapped with the O KLL Auger lines.

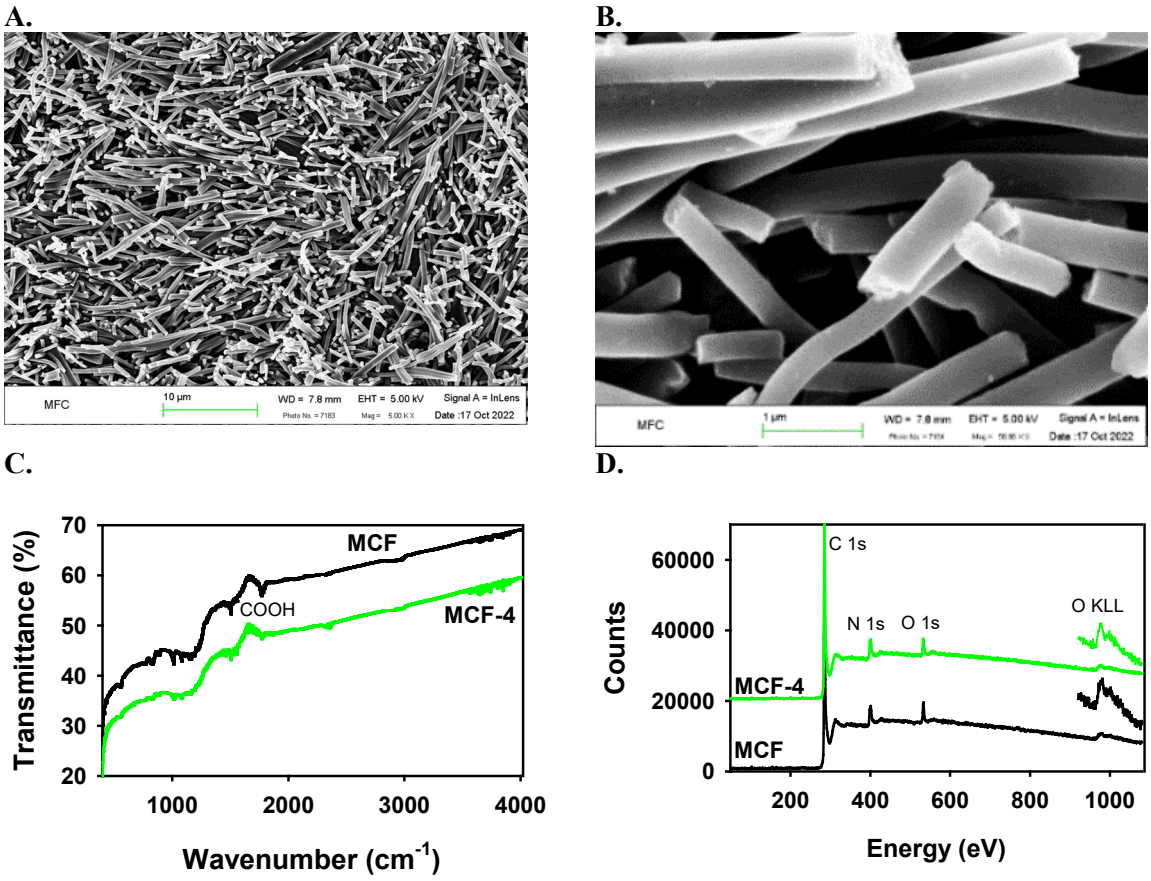

Figure 13. SEM images (A and B) and FTIR spectra (C) and XPS spectra (D) of MCF after Nd adsorption from DI water, in comparison with the spectra of original MCF.

5.2.4 REE Binding Chemistry

In order to understand how Nd is bound with the MCF pores and surfaces, Nd L_3-edge XANES and EXAFS spectra of MCF samples after Nd adsorption were collected at CLS. The Nd L_3-edge XANES spectra of three MCF samples (MCF-2, 3, and 4) after exposure to Nd in DI water (pH 5.5) are shown in **Figure 14A**. The main Nd L_3-edge absorption peak of the MCF samples exposed to Nd was at 6214.5 eV, with a weak feature at about 6226 eV and a broad peak at about 6245 eV. These spectral features were identical to those observed in the Nd L_3-edge XANES spectra of Nd_2O_3, $Nd_2(CO_3)_2$, and Nd doped into calcite,[85] confirming that the Nd chemical species bound in the MCF pores and surfaces was Nd^{3+}.

Nd L_3-edge EXAFS spectra in k-space, Fourier transform plots in R magnitude and real R of these three MCF samples are shown in **Figure 14B, 14C, and 14D**, respectively. The experimental data are shown as dotted lines, and EXAFS fits are shown as colored lines. The fitted EXAFS parameters of these samples are summarized in **Table 1**. The Nd L_3-edge EXAFS data of the MCF samples exposed to Nd were fitted with a Nd-O scattering path at a Nd-O distance of 2.505 ± 0.048 Å with a coordination number of 8.6 ± 0.2 and a Nd-C scattering path at a Nd-C distance of 3.667 ± 0.026 with a coordination number of 2.8 ± 0.3. Including additional scattering paths barely improved their fitting statistics. The EXAFS data fitting of these samples was acceptable as measured by the R factor of 0.015-0.029 (**Table 1**).

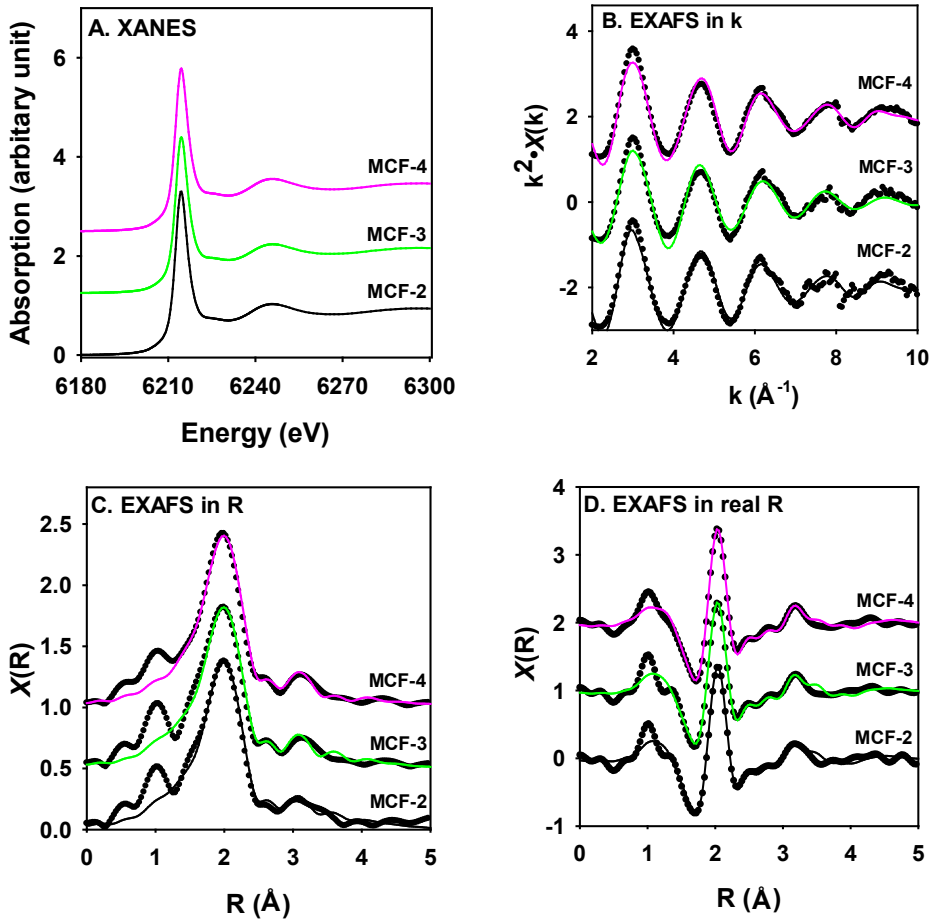

Figure 14. Nd L_3-edge XAS spectra of MCF after Nd adsorption from DI water.

Table 1. Fitting parameters of Nd L_3-edge EXAFS data of MCFs

Samples	Scattering path	Interatomic distance (Å)	Coordination number	Debye–Waller factor, σ^2 (Å^2)	ΔE_0 (eV)	R-factor
MCF-2	Nd-O	2.505 ± 0.014	8.8 ± 1.3	0.0113 ± 0.0029	5.6 ± 0.9	0.0200
	Nd-C	3.652 ± 0.071	2.9 ± 2.9	0.0059 ± 0.0198		
MCF-3	Nd-O	2.553 ± 0.017	8.5 ± 1.5	0.0114 ± 0.0035	6.5 ± 1.1	0.0289
	Nd-C	3.657 ± 0.073	2.3 ± 2.6	0.0014 ± 0.0174		
MCF-4	Nd-O	2.458 ± 0.012	8.5 ± 1.0	0.0110 ± 0.0025	4.2 ± 0.8	0.0151
	Nd-C	3.693 ± 0.052	3.1 ± 2.4	0.0037 ± 0.0141		

The fitted EXAFS parameters for the Nd-O path can be compared with those observed in the Nd-doped calcite (a Nd-O distance of 2.41 Å and a coordination number of 9.5).[85] However, the fitted Nd-C bond distance in the MCF samples were 3.667 Å, much longer than the Nd-C bond distance of 3.26 Å in the Nd-doped calcite, while the fitted Nd-C coordination number in the MCF samples were 2.8, much smaller than the coordination number of 6 in the Nd-doped calcite.[85] Therefore, the Nd-O polyhedron is bounded with the MCF surfaces unlikely as a bidentate mode, a possible explanation for the increased coordination for the larger Nd with a CO_3 group.[85] In addition, the Nd-C bond distance of 3.667 Å, smaller than the Nd-C bond distance of 3.79 Å for ideally linear Nd-O-C connection or corner sharing between Nd-O polyhedron and C-O group. Based on the fitted EXAFS structural parameters of Nd in the MCF samples, a structure model of Nd bound with the MCF surfaces was proposed in **Figure 15**. Nd is coordinated with 8 to 9 oxygen atoms in the Nd-O polyhedron, and the Nd-O polyhedron is connected with 2 carbon atoms in a corner-sharing mode.

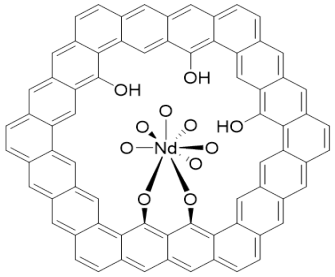

Figure 15. Nd binding structure model with MCF.

In order to further understand how Nd may interact with MCF surfaces, C, N and O K-edge and Nd M-edge XANES spectra of the above samples were also collected at Canadian Light Source and shown in **Figure A5**. The C K-edge XANES spectra (**Figure A5A**) indicated that the C speaks shift to lower energy due to Nd binding and interaction with MCFs, while the Nd M-edge XANES spectra (**Figure A5D**) indicated that the Nd species is trivalent Nd^{3+}, as observed in Nd_2O_3.[86] These results are preliminary, and more research needs to be done.

5.3 DGA- and DTPA-Functionalized MCFs

The FTIR spectrum of DGA-functionalized MCF is shown in **Figure 16A**, in comparison with the FTIR spectra of oxidized MCF and APTS-DGA ligand. For the oxidized MCF, the broad peak at 3300 cm^{-1} is O-H stretching. The peak at 1700 cm^{-1} is C=O stretching. The peak at 1200

cm^{-1} is C-O stretching, indicating that the oxidization step produced hydroxyl groups on the MCF that may react with the coupling agent ATPS for functionalization of DGA. For the ATPS-DGA, the broad peak at 3200 cm^{-1} is N-H stretching. The peak at 1700 cm^{-1} is C=O stretching. The peak at 1000 cm^{-1} is Si-O stretching. The FTIR spectrum shows the condensation between diglycolyl chloride and APTS. Compared with the FTIR spectrum of oxidized MCF, O-H stretching (around 3300 cm^{-1}) on the FTIR spectrum of the DGA-functionalized MCF (MCF-DGA) decreased. The peak at 1700 cm^{-1} is C=O stretching and the peak at 1000 cm^{-1} is Si-O stretching. The FTIR spectra indicated the successful functionalization of DGA ligand on the surface of MCF through the reaction of APTS with the surface hydroxyl groups.

The FTIR spectrum of DTPA-functionalized MCF is shown in **Figure 16B**, in comparison with the FTIR spectra of oxidized MCF and APTS-DTPA ligand. For the APTS-DTPA ligand, the broad peak at 3200 cm^{-1} is N-H stretching. The peak at 1700 cm^{-1} is C=O stretching. The peak at 1000 cm^{-1} is Si-O stretching. The FTIR spectrum shows the condensation between DTPA and APTS. Compared with the FTIR spectrum of oxidized MCF, O-H stretching (around 3300 cm^{-1}) on the FTIR spectrum of the DTPA-functionalized MCF (MCF-DGA) decreased to near zero. The peak at 1700 cm^{-1} is C=O stretching and the peak at 1000 cm^{-1} is Si-O stretching. The FTIR spectra indicated the functionalization of DTPA ligand on the surface of MCF through the reaction of APTS with the surface hydroxyl groups.

Although the successful functionalization of DGA and DTPA onto MCF has been demonstrated, further N_2 adsorption-desorption measurement and SEM characterization indicated that the pore structure of the DGA- and DTPA-functionalized MCF materials were compromised, which might be caused by the strong sulfuric acid and nitric acid (3:1 ratio) used in the oxidation step of MCF. The The new oxidation method of MCF has been developed and new functionalized MCF materials are being prepared accordingly.

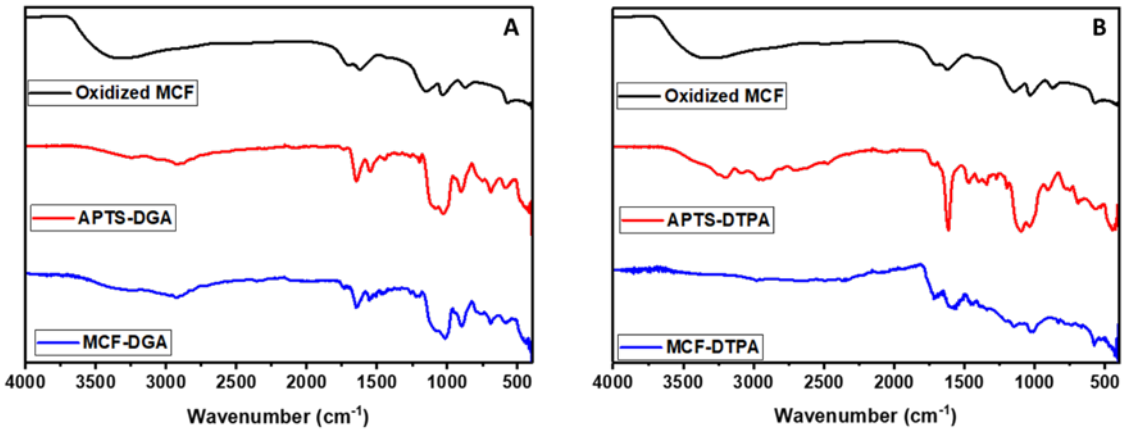

Figure 16. FTIR spectra of DGA- (A) and DTPA-(B) functionalized MCFs.

The DTPA-functionalized MCF material was evaluated for Nd and Pr recovery from a real NdFeB extraction solution, which was prepared under the experimental conditions of 200 mM citrate, pH 1, 200 mL/g of liquid-to-solid ratio, 12 h, and 200 rpm. The chemical compositions of this NdFeB extraction solution are shown in **Table A2**. Major REEs are Nd 963.1 mg/L, Pr 157.4 mg/L, Ce 14.8 mg/L, La 10.5 mg/L, and Dy 0.8 mg/L. Other major elements are Fe 3505.2 mg/L,

B 72.7 mg/L, Co 50.2 mg/L and Al 16.4 mg/L. The Nd and Pr recovery rate and adsorption capacity of this MCF-DTPA are shown in **Table 2**, in comparison with those of MCF without DTPA functionalization. The MCF material was not effective for Nd and Pr recovery from this real NdFeB extraction solution. However, with DTPA functionalization, the MCF-DTPA material exhibited much improved Nd and Pr recovery rates at 23-24%. The amount of Nd adsorbed on MCF-DTPA was 16.5 mg/g, compared to 2.5 mg/g for Pr adsorbed on the MCF-DTPA, essentially in agreement with the Nd and Pr concentrations in the NdFeB extraction solution. These results indicated that MCF-DTPA was equivalently effective for Nd and Pr recovery from the NdFeB extraction solution, but can't separate Nd and Pr.

Table 2. Nd and Pr recovery rate and capacity from real NdFeB citrate extraction solution.

Samples	**Nd**		**Pr**	
	Rate (%)	**Capacity (mg/g)**	**Rate (%)**	**Capacity (mg/g)**
MCF	0	0	0	0
MCF-DTPA	23.5	16.5	23.9	2.5

5.4 Functionalized Mesoporous Silica for REE Recovery

Non-functionalized MMS and phosphonate-functionalized MMS (MMS-PP) were characterized by high and small angle powder XRD, N_2 adsorption isotherms, ^{13}C and ^{31}P CPMAS NMR spectroscopy. The high angle powder XRD patterns of MMS, MMS-PP, and Fe_3O_4 in the range of $2\theta = 10-80°$ are shown in **Figure 17A**, The XRD patterns of both MMS and MMS-PP were characterized with a single broad peak at $2\theta = \sim 20°$, which is consistent with published XRD pattern for MCM-41.[87] The characteristic peaks for Fe_3O_4 are also shown in the XRD patterns of MMS and MMS-PP, confirming that the iron oxide nanoparticles are present inside the core-shell particles.

Small angle XRD patterns for MMS and MMS-PP are shown in **Figure 17B**. The peak (100) at $2\theta \approx 2.3°$ characterizes the hexagonal ordering of the pores in the MCM-41 framework, which is consistent with published data.[76] In addition, two weak peaks corresponding to (110) and (200) at $2\theta = 4\text{-}5°$ were observed in the MMS and MMS-PP patterns. The characteristic (100) peak was shifted slightly toward higher 2θ, and the (110) and (200) peaks became weaker for MMS-PP relative to MMS, indicating that the functionalized phosphonate molecule was primarily grafted into the mesopores and this functionalization slightly altered the hexagonal ordering of the pores in the MCM-41 framework.

The pore size distributions for MMS and MMS-PP were calculated from the N_2 adsorption isotherms (**Figure 17C**) using Barrett-Joyner-Halenda analysis and density functional theory method. The surface area, pore volume, and pore size of MMS were 1010 m^2/g, 0.33 cm^3/g, and 3.3 nm, respectively, while the surface area, pore volume, and pore size of MMS-PP were 512 m^2/g, 0.05 cm^3/g, and 3.0 nm, respectively. The pore volumes and sizes calculated using standard BJH method gave average values for all pores. However, the pore size distribution for the MMS materials calculated using the BJH method was consistent with that of similar magnetic iron oxide/mesoporous silica nanoparticles reported in literature.[76,77] Compared to MMS, the surface area and pore volume of MMS-PP decreased significantly, which indicates that the functionalized molecules were primarily grafted into the mesopores (~3 nm) and less onto external surfaces of

MMS, which is consistent with previously reported data.[76,88] However, the pore size essentially remained unchanged.[76]

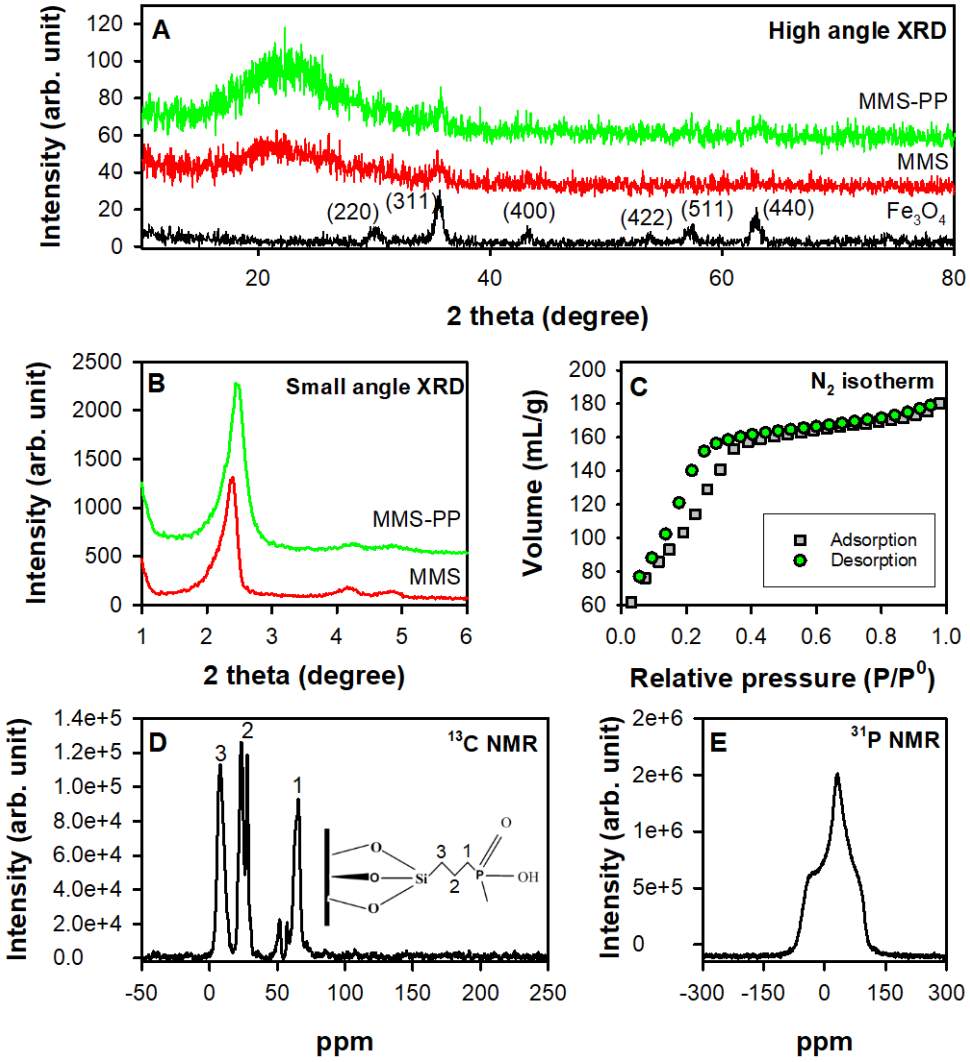

Figure 17. Characterization of phosphonate-functionalized magnetic mesoporous silica (MMS-PP). A. High angle powder XRD, in comparison with non-functionalized MMS and Fe_3O_4, B. Small angle powder XRD, in comparison with MMS, C. N_2 adsorption-desorption isotherms, D. ^{13}C CPMAS NMR spectrum, E. ^{31}P CPMAS NMR spectrum.

The functionalized mesoporous silica (MS-PP) without Fe_3O_4 was analyzed by ^{13}C and ^{31}P CPMAS NMR because Fe_3O_4 in MMS materials interferes with NMR measurements. The ^{13}C CPMAS NMR spectrum of MS-PP is shown in **Figure 17D**. The peak at 65.5 ppm corresponds to carbon 1 (C-O), the peak at 23.3 ppm is attributed to carbon 2 from the propyl chain, and the peak at 7.3 ppm is obtained from carbon 3 (C-Si).[89] The ^{31}P CPMAS NMR spectrum of MS-PP is shown in **Figure 17E**, where the principal peak for phosphonate was at 30.0 ppm, with two spinning side bands at ~100 and ~-40 ppm.[89] Both ^{13}C and ^{31}P NMR spectra of the MS-PP demonstrated that 3-(trihydroxysilyl)propyl methylphosphonate was grafted onto mesoporous silica.

Adsorption isotherms of Nd onto MS-PP and polyethyleneimine-functionalized MMS (MMS-PEI) were obtained from a 50 mM sodium citrate HCl simulant and are shown in **Figure 18A** at an equilibration pH ~2.5 and **Figure 18B** at an equilibration pH ~4.8, in comparison with those of non-functionalized MMS. At pH ~2.5, the maximum Nd adsorption capacity was ~14 mg/g for MMS-PP and ~12 mg/g for MMS-PEI, compared to ~2 mg/g for non-functionalized MMS. At pH ~4.8, the maximum Nd adsorption capacity was ~11 mg/g for MMS-PP and ~9 mg/g for MMS-PEI, compared to 0 mg/g for non-functionalized MMS. Both MMS-PP (**Figure 18C**) and MMS-PEI (**Figure 18D**) remained effective for Nd adsorption from the 50 mM sodium citrate simulant and Nd desorption by 1 M HCl solution after four adsorption-desorption cycles. The Nd adsorption and desorption rates remained at 80-90% for the initial Nd concentration of 5×10^{-4} M. Furthermore, the MMS-PP and MMS-PEI were evaluated for Nd, Pr and Dy recovery from a real NdFeB extraction solution (its chemical compositions could be found in **Table A2**). The Nd, Pr and Dy recovery rates of MMS-PP and MMS-PEI were shown in **Figure 18E**, in comparison with non-functionalized MMS and several functionalized MMS materials (BT - Benzoylthiourea, AD - Polyaryloamidoxime, PPA - Phosphonate-amino, PPI - Poly(propylenimine) dendrimer, and PAMAM - Poly(amidoamine) dendrimer). The results demonstrated that MMS-PP and MMS-PEI were outstanding compared to all other MMS materials.

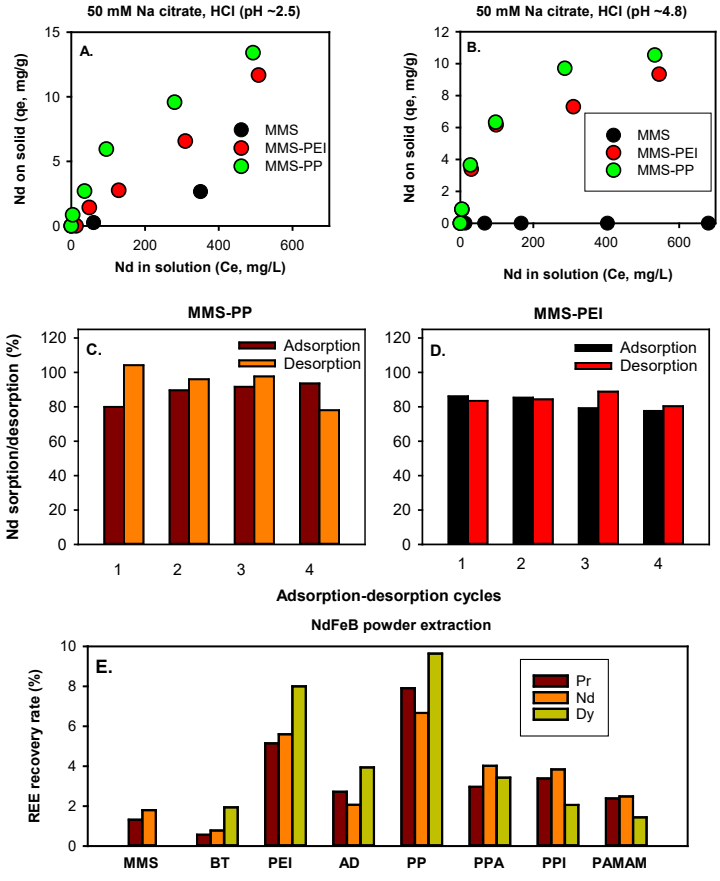

Figure 18. Functionalized magnetic mesoporous silica materials for Nd, Pr and Dy from 50 mM sodium citrate / HCl simulant (A-D) and a real extraction solution of NdFeB powder (E). A and

B. Nd adsorption isotherms of MMS-PP and MMS-PEI (A. pH ~2.5; B. pH ~4.8), C and D. Nd recovery rate after four adsorption-desorption cycles (C. MMS-PP; D. MMS-PEI), E. Nd, Pr, and Dy recovery rate from real extraction solution of NdFeB powder by functionalized MMS.

6 Conclusions and Implications for Future Research

6.1 Conclusions

1. Biodegradable organic ligands (e.g., citrate) can assist the extraction of Nd and Pr from NdFeB powder at pH 2-4 and significantly reduce the use of mineral acids (e.g., HCl) and the generation of new strong acidic waste.

2. Mesoporous carbon fibers (MCF) of surface area 540 m2/g and pore size 10.9 nm were synthesized using PMMA-*b*-PAN block-polymer template, with tunable pore structure, pore size and functionality. MCF exhibited decent Nd adsorption from DI water and 50 mM citric acid simulant, with Nd binding with MCF as corner-sharing mode. For real NdFeB extraction solution of complex chemistry, MCF was not effective for Nd and Pr recovery; however, DTPA functionalized MCF significantly improved Nd and Pr recovery rate and capacity. The used materials can be regenerated for reuse and Nd/Pr harvest.

3. Magnetic mesoporous silica (MMS) has a BET surface area of 1020 m^2/g and pore size of 3.3 nm. Phosphonate (PP)- and polyethyleneimine (PEI) functionalized MMS materials exhibited maximum Nd adsorption capacities of 15 mg/g at pH 2.5 and 10 mg/g at pH 4.8 from 50 mM Na citrate and HCl solutions. The functionalized MMS materials remained effective after four adsorption-desorption cycles. The MMS-PP and MMS-PEI shows significantly improved Nd, Pr and Dy recovery rates from real NdFeB extraction solutions compared to MMS and other functionalized MMS materials.

4. Overall, the acquired proof-of-concept data demonstrated that the advanced mesoporous carbon and silica platform technology potentially enables the REE recovery from magnet scrap and other electronic industrial wastes in environmentally friendly manner, and meanwhile, reduce the management risk and cost of the solid waste streams. Thus, this research will meet the goals of the SERDP Scope of Need (SON) in exploring new sources for domestic REE production, addressing national resource security issues and reducing hazardous solid/liquid waste streams and their environmental risks.

6.2 Future Research

In this **SEED project**, we obtained critical data to demonstrate four key proof-of-concepts: (1) Mesoporous carbon fiber (MCF) materials that are synthesized using our new method with diblock or triblock copolymers as templates, MCF and silica materials are stable in acidic media and tunable in terms of pore size, shape and surface functionalities; (2) Our MCF and silica materials are desirable for the surface functionalization of novel organic ligands into the pores using post-synthesis methods and the mobility of solutions through the fully interconnected pore structures; (3) The new functional MCF and silica materials provide binding sites with selective interactions with REEs, which lead to improved extraction efficiency of Nd, Dy, and Pr from the acidic extracts of a model NdFeB magnet system, effective regeneration of the spent MCF materials for reuse, and downstream Nd, Dy, and Pr recycling; (4) Readily biodegradable and less expensive citrate ligand can promote NdFeB dissolution processes and facilitate REE extraction

at pH 2-4, which can greatly reduce the amount of hydrochloric acid and the generation of new hazardous waste and minimize the environmental impacts. As such, this SEED project provides critical proof-of-concept data for a complete and more comprehensive future study with reduced risk.

The **overarching goal** of the **future research** will be to develop novel functionalized MCF and silica materials as a new platform for effective recovery and separation of REEs from acidic extracts of not only NdFeB magnet scrap, but also other electronic, defensive, and industrial waste streams (**Figure 19**). **Our planned approach** is to use combined rational material design, theoretical computation and machine learning, advanced molecular-level characterization, and robust engineering processes to address this complex system. This combined approach will significantly improve the design of new ligands and our understanding of the driving forces for efficient REE separation. Three focus areas will continue to include the synthesis of stable and tunable MCFs, organic ligand functionalization into the pores, and surface reactivity of the new materials for the extraction and release of REEs. Another potential opportunity is to develop aerogel porous carbon materials for REE recovery. The strategic approach used will integrate experimental methods with computational modeling and machine learning to achieve these objectives. The design, synthesis, and organic ligand functionalization of MCFs will be conducted and optimized based on REE and ligand chemistry, computational modeling and data science, and molecular-level characterization. After thorough characterization, the functionalized MCF materials will be evaluated and optimized for the extraction capacity, selectivity, regeneration for reuse, and downstream REE production from acidic extracts of not only magnet scrap, but also other electronic and industrial waste streams. Computational modeling and machine learning will not only facilitate the selection of ligands and enhance the understanding of REE-ligand interaction mechanisms, but also improve the database and computational models according to experimental data feedback.

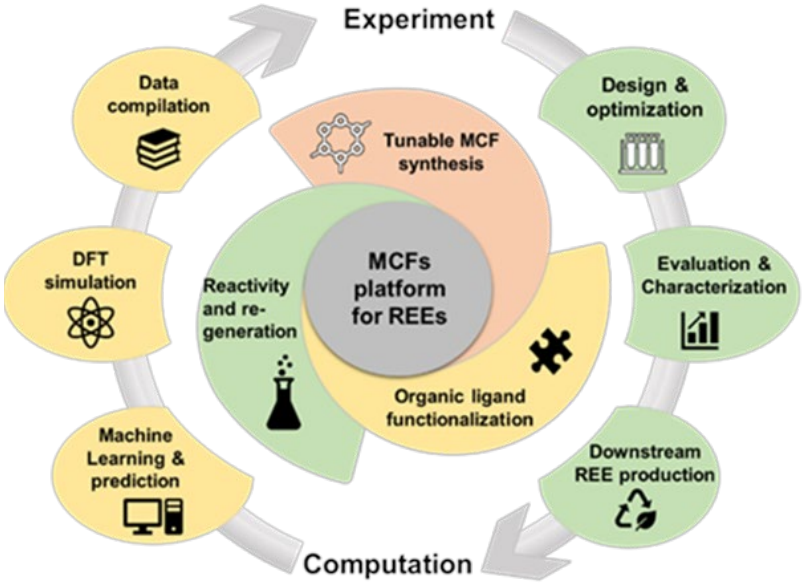

Figure 19. Strategic plan for future research.

The benefits of this robust and environment-friendly technology are two-folded. First, it

can overcome several disadvantages (*e.g.*, high cost, low recovery rate, and a large amount of hazardous/toxic wastes) of traditional hydrometallurgy methods used for REE recovery and separation. Second, it can provide a green, effective, tunable, and potentially universal platform for REE recovery and separation from complex acidic mixtures derived from electronic and industrial wastes as well as mineral ores. As such, the proposed research will advance the DoD and US's capability of securing the future REE material supplies in environmentally sound manners whiling reducing the management risk and remediation cost of electronic and industrial waste streams.

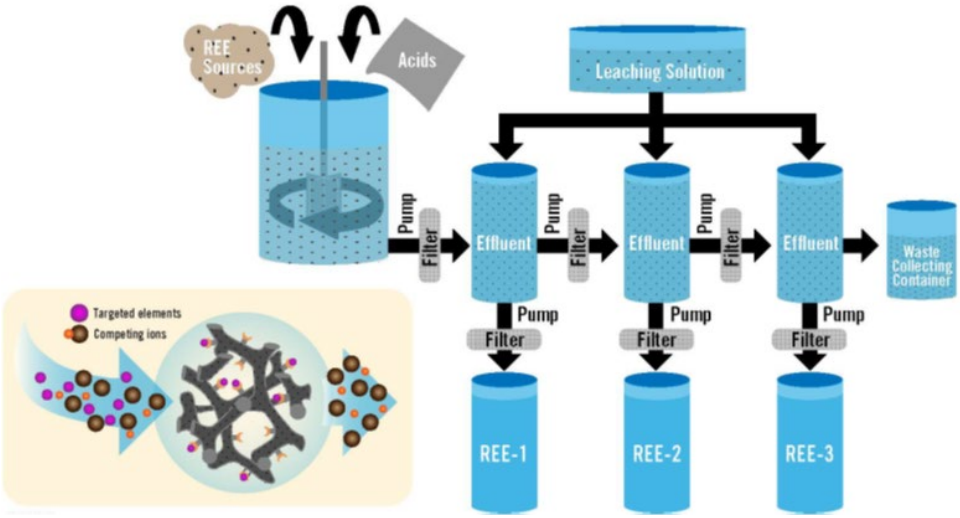

Figure 20. Schematic illustration of a universal separation platform.

In addition to highly controlled surface chemistries, fast mass transport, and short diffusion length with little pressure drop, another important advantage of the proposed MCF materials is the facile scalability of the synthesis and set up for further evaluation in practical applications. A conceptual model is proposed for a potential application of MCF materials as porous traps in a universal separation system (**Figure 20**). The MCF material will be built into the separation system to recover REEs from acidic extracts and release REEs into the concentrates. Since the proposed solid-liquid extraction is based on pumping the leachate through a packed filter, the device performance may vary from the laboratory scale studies due to changes in pressure. However, the unique pore shape and structure of MCFs are expected to facilitate the mobility of leachates through the pores, which will benefit not only the more effective binding of REEs with organic ligands, but also the reduced clog and improved life span of the materials in the real-world applications. Due to the funding and time limits of this seed project, the establishment and evaluation of this platform is not the focus of this seed project. However, it provides a conceptual model that can be tested in a future full proposal.

7 Literature Cited

(1) McGill, I.: Rare Earth Elements. In *Ullmann's Encyclopedia of Industrial Chemistry*; Wiley-VCH: Weinheim, 2000; pp 183-228.

(2) US Department of Energy: *Critical Material Strategy*; U.S. Department of Energy: Washington, D.C., 2010.

(3) US Department of Energy: *Critical Material Strategy*; U.S. Department of Energy: Washington, D.C., 2011.

(4) Van Gosen, B. S.; Verplanck, P. L.; Seal II, R. R.; Long, K. R.; Gambogi, J.: Rare-Earth Elements. In *Critical Mineral Resources of the United States—Economic and Environmental Geology and Prospects for Future Supply*; Schulz, K. J., DeYoung, J., J.H., Seal II, R. R., Bradley, D. C., Eds.; U.S. Geological Survey: Reston, Virginia, 2017.

(5) King, H. M.: *REE - Rare Earth Elements and their Uses*; https://geology.com/articles/rare-earth-elements/, 2020.

(6) US Department of Energy: *Report on Rare Earth Elements from Coal and Coal Byproducts* U.S. Department of Energy: Washington, DC, 2017.

(7) Laboratory, N. E. T.: *Rare Earth Elements - 2019 Project Portfolia, https://netl.doe.gov/coal/rare-earth-elements*; National Energy Technology Laboratory, 2019.

(8) Taggart, R. K.; Hower, J. C.; Dwyer, G. S.; Hsu-Kim, H.: Trends in the Rare Earth Element Content of US-Based Coal Combustion Fly Ashes. *Environmental Science & Technology* **2016**, *50*, 5919-5926.

(9) Yang, Y. X.; Walton, A.; Sheridan, R.; Guth, K.; Gauss, R.; Gutfleisch, O.; Buchert, M.; Steenari, B. M.; Van Gerven, T.; Jones, P. T.; Binnemans, K.: REE Recovery from End-of-Life NdFeB Permanent Magnet Scrap: A Critical Review. *Journal of Sustainable Metallurgy* **2017**, *3*, 122-149.

(10) Chakhmouradian, A. R.; Wall, F.: Rare Earth Elements: Minerals, Mines, Magnets (and More). *Elements* **2012**, *8*, 333-340.

(11) US GAO: Rare Earth Materials: Developing a Comprehensive Approach Could Help DOD Better Manage National Security Risks in the Supply Chain, Report to Congressional Committees, GAO-16-161, 2016

(12) US GAO: Electronic Waste: DOD Is Recovering Materials, but Several Factors May Hinder Near-Term Expansion of These Efforts, Report to Congressional Committees, GAO-16-576, 2016.

(13) Grasso, V. B.: *Rare Earth Elements in National Defense: Background, Oversight Issues, and Options for Congress, Congressional Research Service, R41744*, 2013.

(14) Bonificio, W. D.; Clarke, D. R.: Rare-earth separation using bacteria. *Environmental Science & Technology Letters* **2016**, *3*, 180-184.

(15) Reed, D. W.; Fujita, Y.; Daubaras, A. L.; Jiao, Y.; Thompson, V. S.: Bioleaching of rare earth elements from waste phosphors and cracking catalysts. *Hydrometallurgy* **2016**, *166*, 34-40.

(16) Virolainen, S.; Repo, E.; Sainio, T.: Recovering rare earth elements from phosphogypsum using a resin-in-leach process: Selection of resin, leaching agent, and eluent. *Hydrometallurgy* **2019**, *189*.

(17) Wang, K.; Adidharma, H.; Radosz, M.; Wan, P.; Xu, X.; Russell, C. K.; Tian, H.; Fan, M.; Yu, J.: Recovery of rare earth elements with ionic liquids. *Green Chemistry* **2017**, *19*, 4469-4493.

(18) Singh, S.; Ram, L. C.; Masto, R. E.; Verma, S. K.: A comparative evaluation of minerals and trace elements in the ashes from lignite, coal refuse, and biomass fired power plants. *International Journal of Coal Geology* **2011**, *87*, 112-120.

(19) Taggart, R. K.; Rivera, N. A.; Levard, C.; Ambrosi, J. P.; Borschneck, D.; Hower, J. C.; Hsu-Kim, H.: Differences in bulk and microscale yttrium speciation in coal combustion fly ash. *Environmental Science-Processes & Impacts* **2018**, *20*, 1390-1403.

(20) Walawalkar, M.; Nichol, C. K.; Azirni, G.: An Innovative Process for the Recovery of Consumed Acid in Rare Earth Elements Leaching from Phosphogypsum. *Industrial & Engineering Chemistry Research* **2016**, *55*, 12309-12316.

(21) Deshmane, V. G.; Islam, S. Z.; Bhave, R. R.: Selective Recovery of Rare Earth Elements from a Wide Range of E-Waste and Process Scalability of Membrane Solvent Extraction. *Environmental Science & Technology* **2020**, *54*, 550-558.

(22) Venkatesan, P.; Vander Hoogerstraete, T.; Binnemans, K.; Sun, Z.; Sietsma, J.; Yang, Y. X.: Selective Extraction of Rare-Earth Elements from NdFeB Magnets by a Room-Temperature Electrolysis Pretreatment Step. *Acs Sustainable Chemistry & Engineering* **2018**, *6*, 9375-9382.

(23) Kim, D.; Powell, L. E.; Delmau, L. H.; Peterson, E. S.; Herchenroeder, J.; Bhave, R. R.: Selective Extraction of Rare Earth Elements from Permanent Magnet Scraps with Membrane Solvent Extraction. *Environmental Science & Technology* **2015**, *49*, 9452-9459.

(24) Tian, Y. L.; Liu, Z. W.; Zhang, G. Q.: Recovering REEs from NdFeB wastes with high purity and efficiency by leaching and selective precipitation process with modified agents. *Journal of Rare Earths* **2019**, *37*, 205-210.

(25) Honaker, R. Q.; Zhang, W.; Werner, J.: Acid Leaching of Rare Earth Elements from Coal and Coal Ash: Implications for Using Fluidized Bed Combustion To Assist in the Recovery of Critical Materials. *Energy & Fuels* **2019**, *33*, 5971-5980.

(26) Zhang, W. C.; Honaker, R.: Characterization and recovery of rare earth elements and other critical metals (Co, Cr, Li, Mn, Sr, and V) from the calcination products of a coal refuse sample. *Fuel* **2020**, *267*.

(27) Honaker, R. Q.; Groppo, J.; Yoon, R. H.; Luttrell, G. H.; Noble, A.; Herbst, J.: Process evaluation and flowsheet development for the recovery of rare earth elements from coal and associated byproducts. *Minerals & Metallurgical Processing* **2017**, *34*, 107-115.

(28) Peiravi, M.; Ackah, L.; Guru, R.; Mohanty, M.; Liu, J.; Xu, B.; Zhu, X.; Chen, L.: Chemical extraction of rare earth elements from coal ash. *Minerals & Metallurgical Processing* **2017**, *34*, 170-177.

(29) Smith, R. C.; Taggart, R. K.; Hower, J. C.; Wiesner, M. R.; Hsu-Kim, H.: Selective Recovery of Rare Earth Elements from Coal Fly Ash Leachates Using Liquid Membrane Processes. *Environmental science & technology* **2019**, *53*, 4490-4499.

(30) Ai-Thyabat, S.; Zhang, P.: Extraction of rare earth elements from upgraded phosphate flotation tailings. *Minerals & Metallurgical Processing* **2016**, *33*, 23-30.

(31) Wu, S. X.; Wang, L. S.; Zhao, L. S.; Zhang, P.; El-Shall, H.; Moudgil, B.; Huang, X. W.; Zhang, L. F.: Recovery of rare earth elements from phosphate rock by hydrometallurgical processes - A critical review. *Chemical Engineering Journal* **2018**, *335*, 774-800.

(32) Gergoric, M.; Ravaux, C.; Steenari, B. M.; Espegren, F.; Retegan, T.: Leaching and recovery of rare-earth elements from neodymium magnet waste using organic acids. *Metals* **2018**, *8*.

(33) Lazo, D. E.; Dyer, L. G.; Alorro, R. D.; Browner, R.: Treatment of monazite by organic acids II: Rare earth dissolution and recovery. *Hydrometallurgy* **2018**, *179*, 94-99.

(34) Takahashi, Y.; Kondo, K.; Miyaji, A.; Umeo, M.; Honma, T.; Asaoka, S.: Recovery and Separation of Rare Earth Elements Using Columns Loaded with DNA-filter Hybrid. *Analytical Sciences* **2012**, *28*, 985-992.

(35) Takahashi, Y.; Kondo, K.; Miyaji, A.; Watanabe, Y.; Fan, Q. H.; Honma, T.; Tanaka, K.: Recovery and Separation of Rare Earth Elements Using Salmon Milt. *Plos One* **2014**, *9*.

(36) Auerbach, R.; Bokelmann, K.; Stauber, R.; Gutfleisch, O.; Schnell, S.; Ratering, S.: Critical raw materials - Advanced recycling technologies and processes: Recycling of rare earth metals out of end of life magnets by bioleaching with various bacteria as an example of an intelligent recycling strategy. *Minerals Engineering* **2019**, *134*, 104-117.

(37) Brewer, A.; Dohnalkova, A.; Shutthanandan, V.; Kovarik, L.; Chang, E.; Sawvel, A. M.; Mason, H. E.; Reed, D.; Ye, C. W.; Hynes, W. F.; Lammers, L. N.; Park, D. M.; Jiao, Y. Q.: Microbe Encapsulation for Selective Rare-Earth Recovery from Electronic Waste Leachates. *Environmental Science & Technology* **2019**, *53*, 13888-13897.

(38) Antonick, P. J.; Hu, Z. C.; Fujita, Y.; Reed, D. W.; Das, G.; Wu, L. L.; Shivaramaiah, R.; Kim, P.; Eslamimanesh, A.; Lencka, M. M.; Jiao, Y. Q.; Anderko, A.; Navrotsky, A.; Riman, R. E.: Bio- and mineral acid leaching of rare earth elements from synthetic phosphogypsum Paul. *Journal of Chemical Thermodynamics* **2019**, *132*, 491-496.

(39) Zhou, H. Y.; Wang, Y. L.; Guo, X. G.; Dong, Y. M.; Su, X.; Sun, X. Q.: The recovery of rare earth by a novel extraction and precipitation strategy using functional ionic liquids. *Journal of Molecular Liquids* **2018**, *254*, 414-420.

(40) Wang, K. Y.; Adidharma, H.; Radosz, M.; Wan, P. Y.; Xu, X.; Russell, C. K.; Tian, H. J.; Fan, M. H.; Yu, J.: Recovery of rare earth elements with ionic liquids. *Green Chemistry* **2017**, *19*, 4469-4493.

(41) Pavon, S.; Fortuny, A.; Coll, M. T.; Sastre, A. M.: Rare earths separation from fluorescent lamp wastes using ionic liquids as extractant agents. *Waste Management* **2018**, *82*, 241-248.

(42) Huang, C.; Wang, Y. B.; Huang, B.; Dong, Y. M.; Sun, X. Q.: The recovery of rare earth elements from coal combustion products by ionic liquids. *Minerals Engineering* **2019**, *130*, 142-147.

(43) Dupont, D.; Binnemans, K.: Recycling of rare earths from NdFeB magnets using a combined leaching/extraction system based on the acidity and thermomorphism of the ionic liquid Hbet Tf2N. *Green Chemistry* **2015**, *17*, 2150-2163.

(44) Davris, P.; Balomenos, E.; Panias, D.; Paspaliaris, I.: Selective leaching of rare earth elements from bauxite residue (red mud), using a functionalized hydrophobic ionic liquid. *Hydrometallurgy* **2016**, *164*, 125-135.

(45) Makanyire, T.; Sanchez-Segado, S.; Jha, A.: Separation and recovery of critical metal ions using ionic liquids. *Advances in Manufacturing* **2016**, *4*, 33-46.

(46) Kitagawa, J.; Uemura, R.: Rare Earth Extraction from NdFeB Magnet Using a Closed-Loop Acid Process. *Scientific Reports* **2017**, *7*.

(47) Gergoric, M.; Ekberg, C.; Steenari, B. M.; Retegan, T.: Separation of heavy rare-earth elements from light rare-earth elements via solvent extraction from a neodymium magnet leachate and the effects of diluents. *Journal of Sustainable Metallurgy* **2017**, *3*, 601-610.

(48) Kumari, A.; Sahu, K. K.; Sahu, S. K.: Solvent Extraction and Separation of Nd, Pr and Dy from Leach Liquor of Waste NdFeB Magnet Using the Nitrate Form of Mextral (R) 336At in the Presence of Aquo-Complexing Agent EDTA. *Metals* **2019**, *9*.

(49) Sethurajan, M.; van Hullebusch, E. D.; Fontana, D.; Akcil, A.; Deveci, H.; Batinic, B.; Leal, J. P.; Gasche, T. A.; Kucuker, M. A.; Kuchta, K.; Neto, I. F. F.; Soares, H.; Chmielarz, A.: Recent advances on hydrometallurgical recovery of critical and precious elements from end of life electronic wastes-a review. *Critical Reviews in Environmental Science and Technology* **2019**, *49*, 212-275.

(50) Tunsu, C.; Petranikova, M.; Gergoric, M.; Ekberg, C.; Retegan, T.: Reclaiming rare earth elements from end-of-life products: A review of the perspectives for urban mining using hydrometallurgical unit operations. *Hydrometallurgy* **2015**, *156*, 239-258.

(51) Ding, Y.; Harvey, D.; Wang, N. H. L.: Two-zone ligand-assisted displacement chromatography for producing high-purity praseodymium, neodymium, and dysprosium with high yield and high productivity from crude mixtures derived from waste magnets. *Green Chemistry* **2020**, *22*, 3769-3783.

(52) Itoh, M.; Miura, K.; Machida, K.: Novel rare earth recovery process on Nd-Fe-B magnet scrap by selective chlorination using NH4Cl. *Journal of Alloys and Compounds* **2009**, *477*, 484-487.

(53) Hua, Z. S.; Wang, J.; Wang, L.; Zhao, Z.; Li, X. L.; Xiao, Y. P.; Yang, Y. X.: Selective Extraction of Rare Earth Elements from NdFeB Scrap by Molten Chlorides. *Acs Sustainable Chemistry & Engineering* **2014**, *2*, 2536-2543.

(54) Makarova, I.; Soboleva, E.; Osipenko, M.; Kurilo, I.; Laatikainen, M.; Repo, E.: Electrochemical leaching of rare-earth elements from spent NdFeB magnets. *Hydrometallurgy* **2020**, *192*.

(55) Liu, C. Y.; Yan, Q. B.; Zhang, X. W.; Lei, L. C.; Xiao, C. L.: Efficient recovery of end-of-life NdFeB permanent magnets by selective leaching with deep eutectic solvents. *Environmental Science & Technology* **2020**, *54*, 10370-10379.

(56) Fryxell, G. E.; Mattigod, S. V.; Lin, Y. H.; Wu, H.; Fiskum, S.; Parker, K.; Zheng, F.; Yantasee, W.; Zemanian, T. S.; Addleman, R. S.; Liu, J.; Kemner, K.; Kelly, S.; Feng, X. D.: Design and synthesis of self-assembled monolayers on mesoporous supports (SAMMS): The importance of ligand posture in functional nanomaterials. *Journal of Materials Chemistry* **2007**, *17*, 2863-2874.

(57) Fryxell, G. E.; Lin, Y. H.; Fiskum, S.; Birnbaum, J. C.; Wu, H.; Kemner, K.; Kelly, S.: Actinide sequestration using self-assembled monolayers on mesoporous supports. *Environmental Science & Technology* **2005**, *39*, 1324-1331.

(58) Florek, J.; Giret, S.; Juere, E.; Lariviere, D.; Kleitz, F.: Functionalization of mesoporous materials for lanthanide and actinide extraction. *Dalton Transactions* **2016**, *45*, 14832-14854.

(59) Florek, J.; Chalifour, F.; Bilodeau, F.; Lariviere, D.; Kleitz, F.: Nanostructured hybrid materials for the selective recovery and enrichment of rare earth elements. *Advanced Functional Materials* **2014**, *24*, 2668-2676.

(60) Hu, Y. M.; Florek, J.; Lariviere, D.; Fontaine, F. G.; Kleitz, F.: Recent advances in the separation of rare earth elements using mesoporous hybrid materials. *Chemical Record* **2018**, *18*, 1261-1276.

(61) Zheng, X. D.; Wang, C.; Dai, J. D.; Shi, W. D.; Yan, Y. S.: Design of mesoporous silica hybrid materials as sorbents for the selective recovery of rare earth metals. *Journal of Materials Chemistry A* **2015**, *3*, 10327-10335.

(62) Zhang, W. Z.; Avdibegovic, D.; Koivula, R.; Hatanpaa, T.; Hietala, S.; Regadio, M.; Binnemans, K.; Harjula, R.: Titanium alkylphosphate functionalised mesoporous silica for enhanced uptake of rare-earth ions. *Journal of Materials Chemistry A* **2017**, *5*, 23805-23814.

(63) Ramasamy, D. L.; Repo, E.; Srivastava, V.; Sillanpaa, M.: Chemically immobilized and physically adsorbed PAN/acetylacetone modified mesoporous silica for the recovery of rare earth elements from the waste water-comparative and optimization study. *Water Research* **2017**, *114*, 264-276.

(64) Hu, Y. M.; Castro, L. C. M.; Drouin, E.; Florek, J.; Kahlig, H.; Lariviere, D.; Kleitz, F.; Fontaine, F. G.: Size-selective separation of rare earth elements using functionalized mesoporous silica materials. *Acs Applied Materials & Interfaces* **2019**, *11*, 23681-23691.

(65) Callura, J. C.; Perkins, K. M.; Noack, C. W.; Washburn, N. R.; Dzombak, D. A.; Karamalidis, A. K.: Selective adsorption of rare earth elements onto functionalized silica particles. *Green Chemistry* **2018**, *20*, 1515-1526.

(66) Perreault, L. L.; Giret, S.; Gagnon, M.; Florek, J.; Lariviere, D.; Kleitz, F.: Functionalization of Mesoporous Carbon Materials for Selective Separation of Lanthanides under Acidic Conditions. *Acs Applied Materials & Interfaces* **2017**, *9*, 12003-12012.

(67) Bertelsen, E. R.; Deodh, G.; Kluherz, K. T.; Davidson, M.; Adams, M. L.; Trewyn, B. G.; Shafer, J. C.: Microcolumn lanthanide separation using bis-(2-ethylhexyl)phosphoric acid functionalized ordered mesoporous carbon materials. *Journal of Chromatography A* **2019**, *1595*, 248–256.

(68) Liang, C. D.; Li, Z. J.; Dai, S.: Mesoporous carbon materials: Synthesis and modification. *Angewandte Chemie-International Edition* **2008**, *47*, 3696-3717.

(69) Han, S. J.; Sohn, K.; Hyeon, T.: Fabrication of new nanoporous carbons through silica templates and their application to the adsorption of bulky dyes. *Chemistry of Materials* **2000**, *12*, 3337-3341.

(70) Zhou, Z. P.; Liu, T. Y.; Khan, A. U.; Liu, G. L.: Block copolymer-based porous carbon fibers. *Science Advances* **2019**, *5*, eaau6852.

(71) Liu, T.; Serrano, J.; Elliott, J.; Yang, X.; Cathcart, W.; Wang, Z.; He, Z.; Liu, G. L.: Exceptional capacitive deionization rate and capacity by block copolymer–based porous carbon fibers. *Science Advances* **2020**, *6*, eaaz0906.

(72) Serrano, J. M.; Khan, A. U.; Liu, T. Y.; Xu, Z.; Esker, A. R.; Liu, G. L.: Capacitive Organic Dye Removal by Block Copolymer Based Porous Carbon Fibers. *Advanced Materials Interfaces* **2020**, 2000507.

(73) Liu, T. Y.; Zhou, Z. P.; Guo, Y. C.; Guo, D.; Liu, G. L.: Block copolymer derived uniform mesopores enable ultrafast electron and ion transport at high mass loadings. *Nature Communications* **2019**, *10*, 675.

(74) Werner, E. J.; Biros, S. M.: Supramolecular ligands for the extraction of lanthanide and actinide ions. *Organic Chemistry Frontiers* **2019**, *6*, 2067-2094.

(75) Lin, Y. S.; Haynes, C. L.: Synthesis and characterization of biocompatible and size-tunable multifunctional porous silica nanoparticles. *Chemistry of Materials* **2009**, *21*, 3979-3986.

(76) Egodawatte, S.; Datt, A.; Burns, E. A.; Larsen, S. C.: Chemical insight into the adsorption of chromium(III) on iron oxide/mesoporous silica nanocomposites. *Langmuir* **2015**, *31*, 7553-7562.

(77) Knezevic, N. Z.; Slowing, I. I.; Lin, V. S. Y.: Tuning the release of anticancer drugs from magnetic iron oxide/mesoporous silica core/shell nanoparticles. *Chempluschem* **2012**, *77*, 48-55.

(78) Vivero-Escoto, J. L.; Carboni, M.; Abney, C. W.; deKrafft, K. E.; Lin, W. B.: Organo-functionalized mesoporous silicas for efficient uranium extraction. *Microporous and Mesoporous Materials* **2013**, *180*, 22-31.

(79) Xu, X. C.; Song, C. S.; Andresen, J. M.; Miller, B. G.; Scaroni, A. W.: Novel polyethylenimine-modified mesoporous molecular sieve of MCM-41 type as high-capacity adsorbent for CO2 capture. *Energy & Fuels* **2002**, *16*, 1463-1469.

(80) Ravel, B.; Newville, M.: Athena, Artemis, Hephaestus: data analysis for X-ray absorption spectroscopy using IFEFFIT. *J. Synchrotron Radiat.* **2005**, *12*, 537−541.

(81) Ni, Y. X.; Hughes, J. M.; Mariano, A. N.: The atomic arrangement of bastnisite-(Ce), $Ce(CO_3)F$, and structural elements of synchysite-(Ce), riintgenite-(Ce), and parisite-(Ce). *American Mineralogist* **1993**, *78*, 415-418.

(82) Regier, T.; Krochak, J.; Sham, T. K.; Hu, Y. F.; Thompson, J.; Blyth, R. I. R.: Performance and capabilities of the Canadian Dragon: The SGM beamline at the Canadian Light Source. *Nuclear Instruments & Methods in Physics Research Section a-Accelerators Spectrometers Detectors and Associated Equipment* **2007**, *582*, 93-95.

(83) Gillespie, A. W.; Phillips, C. L.; Dynes, J. J.; Chevrier, D.; Regier, T. Z.; Peak, D.: Advances in Using Soft X-Ray Spectroscopy for Measurement of Soil Biogeochemical Processes. In *Advances in Agronomy*; Sparks, D. L., Ed.; Academic Press., 2015; pp 1-32.

(84) Solomon, D.; Lehmann, J.; Kinyangi, J.; Liang, B. Q.; Heymann, K.; Dathe, L.; Hanley, K.; Wirick, S.; Jacobsen, C.: Carbon (1s) NEXAFS Spectroscopy of Biogeochemically Relevant Reference Organic Compounds. *Soil Science Society of America Journal* **2009**, *73*, 1817-1830.

(85) Elzinga, E. J.; Reeder, R. J.; Withers, S. H.; Peale, R. E.; Mason, R. A.; Beck, K. M.; Hess, W. P.: EXAFS study of rare-earth element coordination in calcite. *Geochimica et Cosmochimica Acta* **2002**, *66*, 2875–2885.

(86) Rai, V. N.; Rajput, P.; Jha, S. N.; Bhattacharyya, D.; Raja Shekhar, B. N.; Deshpanded, U. P.; Shripathid, T.: Effect of gamma irradiation on X-ray absorption and photoelectron spectroscopy of Nd-doped phosphate glass. *Journal of Synchrotron Radiation* **2016**, *23*, 1424–1432.

(87) Kaya, E.; Oktar, N.; Karakas, G.; Murtezaoglu, K.: Synthesis and characterization of Ba/MCM-41. *Turk. J. Chem.* **2010**, *34*, 935-943.

(88) Datt, A.; El-Maazawi, I.; Larsen, S. C.: Aspirin loading and release from MCM-41 functionalized with aminopropyl groups via co-condensation or postsynthesis modification methods. *Journal of Physical Chemistry C* **2012**, *116*, 18358-18366.

(89) Hernández-Velázquez, P. I.; Gutiérrez-Ortega, H. A.; CarbajalArizaga, G. G.; Manríquez-González, R.; De la Cruz-Hernández, W.; Gómez-Salazar, S.: Hybrid functionalized phosphonate silica: Insight into chromium removal chemistry from aqueous solutions. *J. Mex. Chem. Soc.* **2019**, *63*, 130-153.

8 Appendices

Table A1. Chemical compositions of NdFeB powder.

REEs				Other elements		
Element	**Concentration (mg/kg)**	**Mass (wt%)**		**Element**	**Concentration (mg/kg)**	**Mass (wt%)**
Sc	0.00	0.00		Al	3278.42	0.33
Y	0.00	0.00		Fe	698463.62	69.85
La	**2502.79**	**0.25**		B	14529.54	1.45
Ce	**3850.26**	**0.39**		Co	10036.93	1.00
Pr	**34785.63**	**3.48**		K	1282.67	0.13
Nd	**223620.46**	**22.36**		Si	905.74	0.09
Sm	27.87	0.00		Sr	859.27	0.09
Eu	0.00	0.00		Cr	414.01	0.04
Gd	935.99	0.09		Cu	410.27	0.04
Tb	117.43	0.01		Mn	214.13	0.02
Dy	39.04	0.00		Mo	80.13	0.01
Ho	4.69	0.00		Ti	69.43	0.01
Er	154.15	0.02		Ni	64.33	0.01
Tm	0.00	0.00		Zn	14.18	0.00
Yb	0.00	0.00		Cd	1.26	0.00
Lu	0.00	0.00		Ba	4.86	0.00

Table A2. Chemical compositions of NdFeB extraction solution.

REEs			Other elements	
Element	**Concentration (mg/L)**		**Element**	**Concentration (mg/L)**
Sc	0.00		**Al**	**16.39**
Y	0.00		**Fe**	**3505.19**
La	**10.51**		**B**	**72.65**
Ce	**14.75**		**Co**	**50.18**
Pr	**157.43**		K	6.41
Nd	**963.10**		Si	4.53
Sm	0.29		Sr	4.30
Eu	0.00		Cr	2.07
Gd	5.98		Cu	2.05
Tb	0.84		Mn	1.07
Dy	0.75		Mo	0.40
Ho	0.10		Ti	0.35
Er	0.97		Ni	0.32
Tm	0.00		Zn	0.07
Yb	0.00			
Lu	0.00			

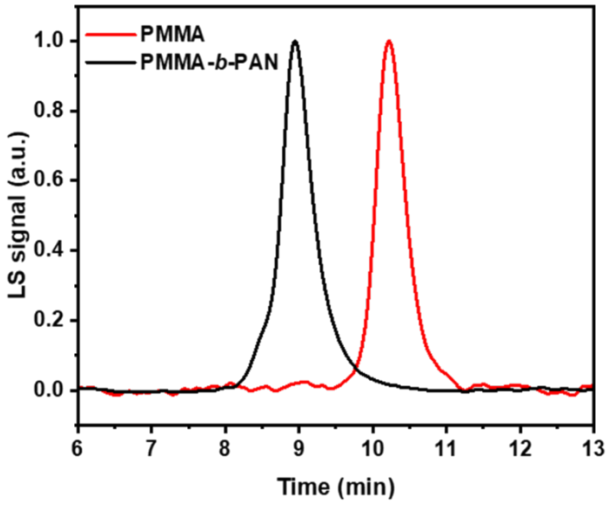

Figure A1. The size exclusion chromatography traces of PMMA and PMMA-*b*-PAN block copolymer.

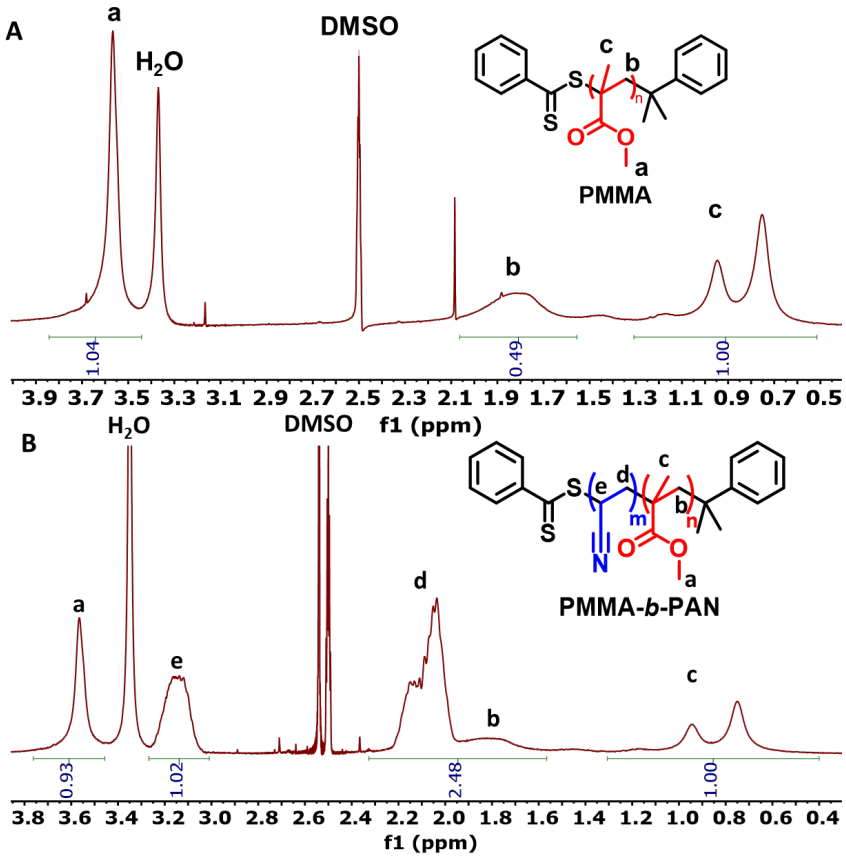

Figure A2. [1]H NMR spectra of PMMA (A) and PMMA-b-PAN (B) block copolymer.

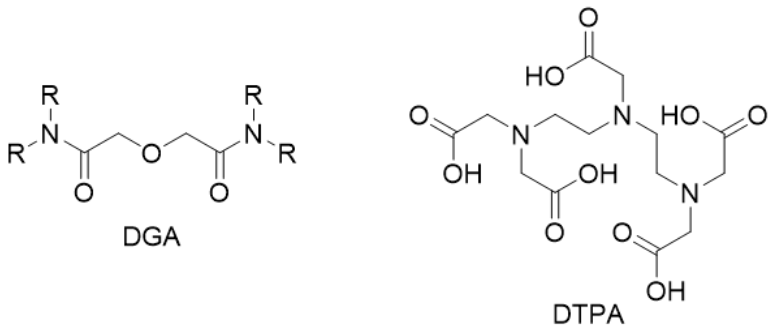

Figure A3. Structure of ligands selected and synthesized for REEs extraction.

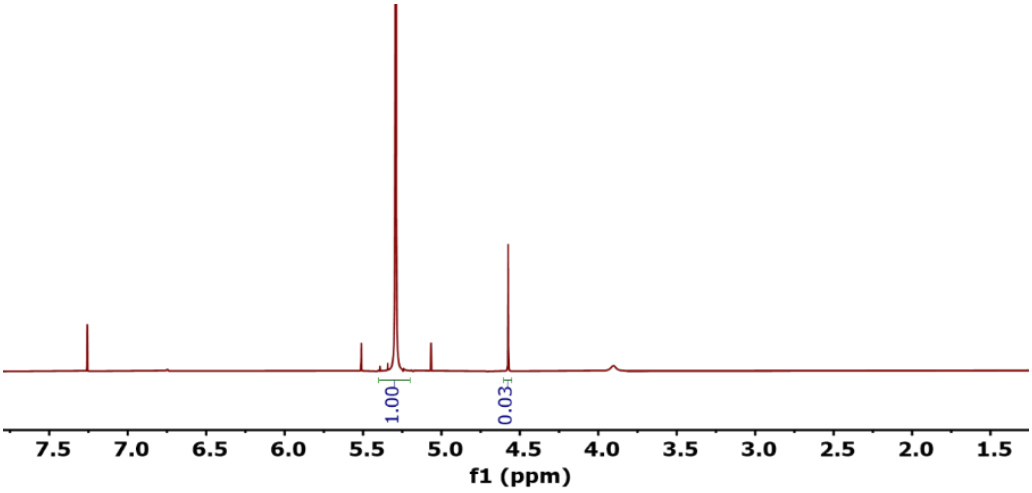

Figure A4. ^{1}H NMR spectrum of diglycolyl chloride.

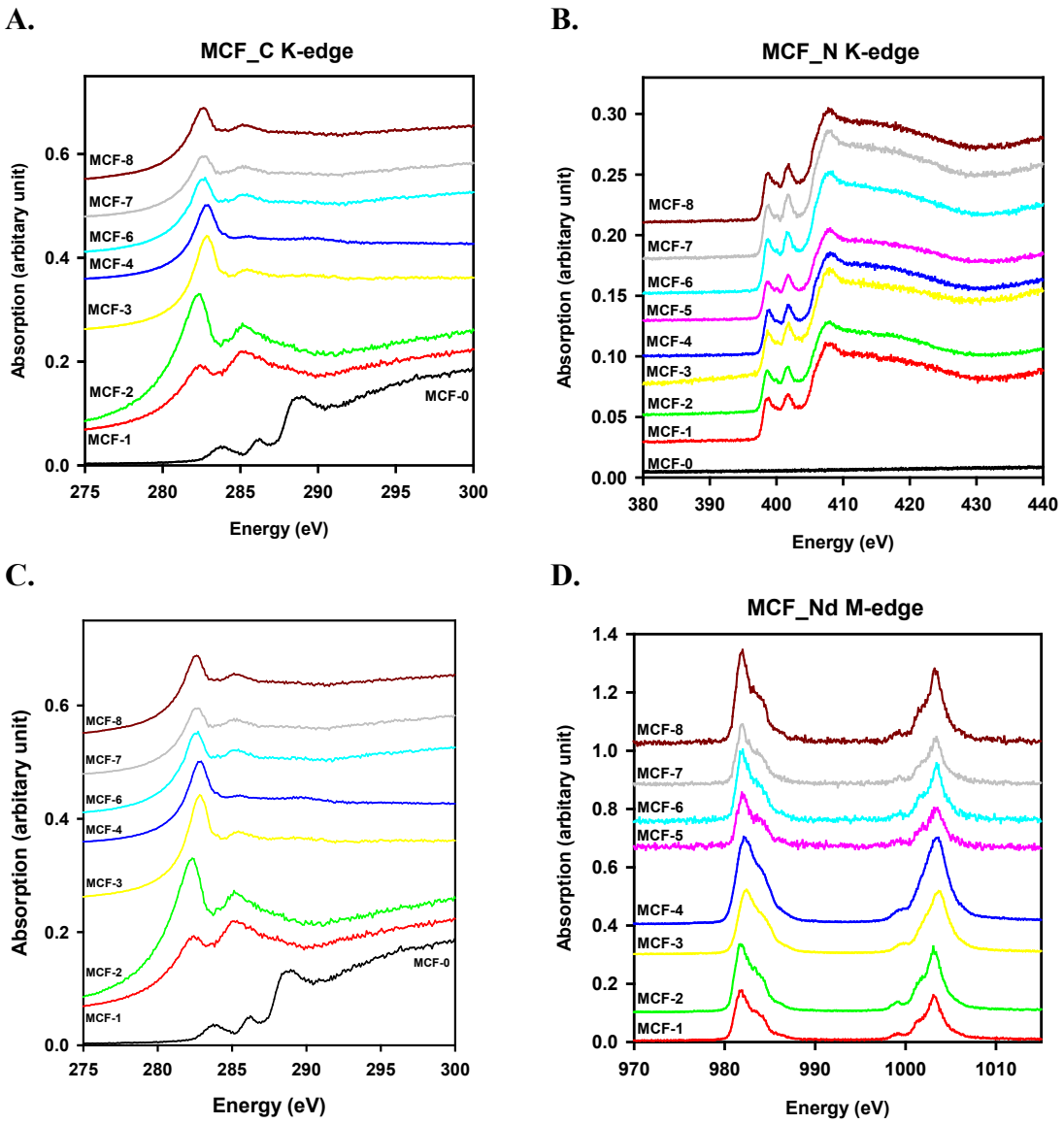

Figure A5. Carbon (A), nitrogen (B) and oxygen (C) K-edge and Nd M-edge (D) XANES spectra of MCFs with Nd adsorption.